Article

Cell

Centromeres License the Mitotic Condensation of Yeast Chromosome Arms

Graphical Abstract

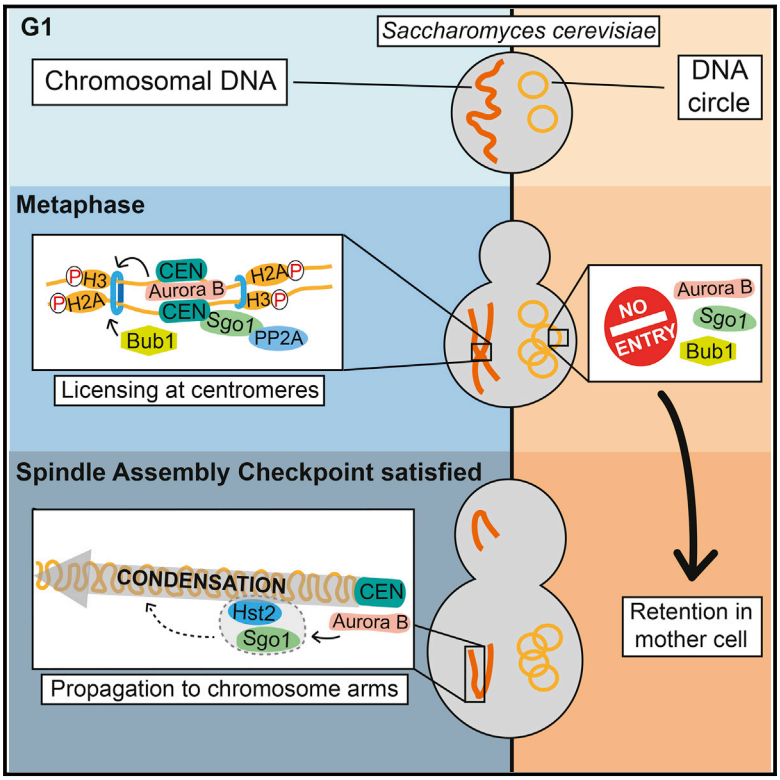

Highlights

- Yeast chromosomes autonomously condense in a centromere-dependent manner
- The condensation signal is triggered by centromeric Aurora B in late metaphase
- Shugoshin promotes the spreading of this signal to chromosome arms
- Centromere-less chromatin fails to condense, preventing its mitotic propagation

Authors

Tom Kruitwagen, Pierre Chymkowitch, Annina Denoth-Lippuner, Jorrit Enserink, Yves Barral

Correspondence

yves.barral@bc.biol.ethz.ch

In Brief

Yeast centromeres propagate a *cis*-acting chromosome condensation signal.

Kruitwagen et al., 2018, Cell *175*, 1–16
October 18, 2018
https://doi.org/10.1016/j.cell.2018.09.012

CellPress

Please cite this article in press as: Kruitwagen et al., Centromeres License the Mitotic Condensation of Yeast Chromosome Arms, Cell (2018), https://doi.org/10.1016/j.cell.2018.09.012

Article

Cell

Centromeres License the Mitotic Condensation of Yeast Chromosome Arms

Tom Kruitwagen,[1,5] Pierre Chymkowitch,[2,5,7] Annina Denoth-Lippuner,[1,6] Jorrit Enserink,[2,3,4] and Yves Barral[1,8,*]
[1]Institute of Biochemistry, Biology Department, ETH Zurich, 8093 Zurich, Switzerland
[2]Department of Molecular Cell Biology, Institute for Cancer Research, Oslo University Hospital, Montebello, 0379 Oslo, Norway
[3]Faculty of Medicine, Center for Cancer Cell Reprogramming, Institute of Clinical Medicine, University of Oslo, Oslo, Norway
[4]Faculty of Mathematics and Natural Sciences, Department of Biosciences, University of Oslo, Norway
[5]These authors contributed equally
[6]Present address: Brain Research Institute, Faculty of Medicine and Science, University of Zurich, 8057 Zurich, Switzerland
[7]Present address: Department of Microbiology, Oslo University Hospital, Sognsvannsveien 20, 0027 Oslo, Norway
[8]Lead Contact
*Correspondence: yves.barral@bc.biol.ethz.ch
https://doi.org/10.1016/j.cell.2018.09.012

SUMMARY

During mitosis, chromatin condensation shapes chromosomes as separate, rigid, and compact sister chromatids to facilitate their segregation. Here, we show that, unlike wild-type yeast chromosomes, non-chromosomal DNA circles and chromosomes lacking a centromere fail to condense during mitosis. The centromere promotes chromosome condensation strictly in *cis* through recruiting the kinases Aurora B and Bub1, which trigger the autonomous condensation of the entire chromosome. Shugoshin and the deacetylase Hst2 facilitated spreading the condensation signal to the chromosome arms. Targeting Aurora B to DNA circles or centromere-ablated chromosomes or releasing Shugoshin from PP2A-dependent inhibition bypassed the centromere requirement for condensation and enhanced the mitotic stability of DNA circles. Our data indicate that yeast cells license the chromosome-autonomous condensation of their chromatin in a centromere-dependent manner, excluding from this process non-centromeric DNA and thereby inhibiting their propagation.

INTRODUCTION

During mitosis, chromosome condensation promotes decatenation of sister chromatids from each other, shortening of chromosome arms, and reshaping chromatids into segregable units (Piskadlo and Oliveira, 2016; Antonin and Neumann, 2016; Neurohr et al.,2011; Kruitwagen et al., 2015). However, we know little about how the orderly condensation of chromosomes is orchestrated and how it is coordinated with other mitotic events, such as chromosome attachment to the mitotic spindle and the subsequent resolution of chromosome cohesion.

Saccharomyces cerevisiae emerged as a system of choice to study these questions. Its nuclear genome is ~12 mega base pairs (MBps) long and distributed over 16 linear chromosomes. Each contains a short, point centromere, where a single centromeric nucleosome forms and recruits the kinetochore (Biggins, 2013; Marston, 2014). Beyond attaching chromosomes to the mitotic spindle, the centromere carries out additional functions, such as sensing and signaling the attachment status of the sister chromatids to the spindle during metaphase and halting progression to anaphase until every single chromosome is bipolarly attached to the spindle. Interestingly, it also promotes the recruitment of cohesin, condensin, and associated signaling molecules to pericentromeric regions, which show a specialized chromatin composition and structure (Stephens et al., 2011; Biggins, 2013). On one side, maintaining proper cohesion of sister centromeres is essential to establish and sense proper, bipolar spindle attachment of sister kinetochores. On the other side, some of these pericentromeric components, such as condensin and the chromosomal passenger complex, are also involved in chromosome condensation. However, whether these two functions are related to each other is unknown.

Chromosome condensation includes several processes, particularly the contraction of chromosome arms (Antonin and Neumann, 2016; Kschonsak and Haering, 2015; Vas et al., 2007) and the compaction of chromatin fibers by nucleosome-nucleosome interaction (Kruitwagen et al., 2015; Wilkins et al., 2014). Although condensation is well visible on large chromosomes of plants and metazoans, it is difficult to monitor on much smaller yeast chromosomes. In this organism, shortening of the spatial distance between two fluorescently labeled loci is a measure of chromosome arm contraction (henceforth called contraction) (Neurohr et al., 2011; Vas et al., 2007). Nucleosome-nucleosome interaction cannot be resolved by diffraction-limited microscopy, but this is overcome owing to chromatin compaction (henceforth called so) bringing associated fluorophores within fluorescence resonance energy transfer (FRET) (when using two fluorophores) or quenching distances (when using a single fluorophore) (Kruitwagen et al., 2015). To characterize the role of centromeric factors on chromosome condensation, we used these methods and characterized the state of centromeric and non-centromeric chromatin during yeast mitosis.

Please cite this article in press as: Kruitwagen et al., Centromeres License the Mitotic Condensation of Yeast Chromosome Arms, Cell (2018), https://doi.org/10.1016/j.cell.2018.09.012

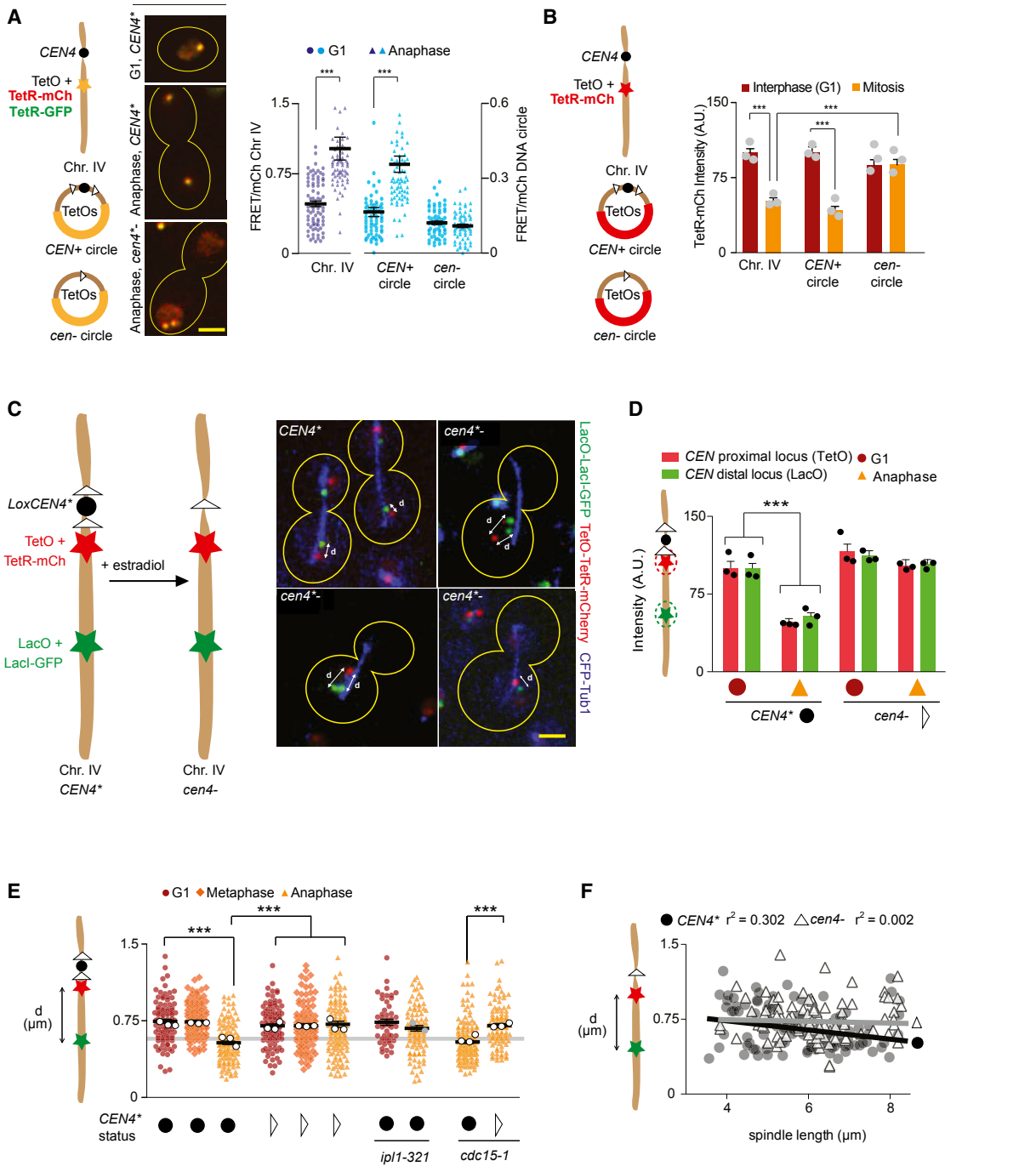

Figure 1. Non-centromeric DNA Does Not Condense

(A) An array of 256 TetO repeats is inserted in the indicated DNA molecules (left) in cells co-expressing TetR-mCherry and TetR-GFP, leading to a fluorescent focus at the tagged locus (images of cells with indicated phenotype and cell-cycle stage). FRET intensity (see the STAR Methods) at the foci on the indicated molecules and cell-cycle stage (right).

(B) Fluorescence intensity of TetR-mCherry foci (inversely correlated to compaction) on the indicated molecules and cell-cycle stages.

(C) Estradiol-inducible formation of the *cen4*− reporter chromosome (left) and representative *CEN4+* or *cen4*− anaphase cells. The measured distances are shown (white arrows, d).

(D) Fluorescence intensities of indicated loci and genotypes in G1 and anaphase mother cells.

(E) *TRP1-LYS4* distance (contraction) of *CEN4** (black circle) and *cen4*− (white triangle) chr IV in the indicated cell-cycle stages and perturbations.

(F) Plot of anaphase *TRP1-LYS4* distances (μm) as a function of spindle length for *CEN4** and *cen4*− chromosomes. The trends (linear regression) and R^2 values are indicated.

(legend continued on next page)

Please cite this article in press as: Kruitwagen et al., Centromeres License the Mitotic Condensation of Yeast Chromosome Arms, Cell (2018), https://doi.org/10.1016/j.cell.2018.09.012

RESULTS

DNA Circles Do Not Condense during Mitosis

We first tested whether the chromatin of *CEN+* and *cen−* circles behaves similarly in mitosis. These are too small to measure axial contraction. Hence, we tested chromatin compaction by measuring FRET between TetR-mCherry and TetR-GFP molecules bound to an array of 224 Tet operator sequences (TetO) placed on either the right arm of chromosome IV (chr IV) or a model, self-replicating DNA circle (Denoth-Lippuner et al., 2014b; Shcheprova et al., 2008) (Figure 1A). On chr IV and on a *CEN+* circle, compaction led to increased FRET as the cells enter anaphase, compared to cells in interphase (G1) (Figure 1A), as previously reported (Kruitwagen et al., 2015). Similarly, cells expressing only TetR-mCherry showed decreased fluorescence intensity at these TetO arrays during mitosis, due to quenching of neighboring fluorophores (Figure 1B) (Kruitwagen et al., 2015). In sharp contrast, both FRET and quenching remained constitutively low over the cell cycle on *cen−* DNA circles (Figures 1A and 1B), indicating that they failed to condense in mitosis. These first data indicated that unlike chromosomal chromatin, non-chromosomal chromatin did not compact during mitosis, despite being in the same nucleus. Remarkably, these data also suggested that adding a centromere was sufficient to instruct chromatin to compact. Thus, *cen−* and *CEN+* chromatin behave differently in mitosis.

Non-centromeric Chromosomes Do Not Condense in Mitosis

Building on these observations, we wondered whether centromeres generally instruct bona fide chromosomes to condense in mitosis. We flanked the centromere of chr IV, the second longest chromosome in yeast, with *lox* recombination sites to allow its excision (forming *CEN4**) (Warsi et al., 2008) (see the STAR Methods). Consistently, when expressing Cre recombinase fused to an estradiol-binding domain (Cre-EBD) (Lindstrom and Gottschling, 2009) (Figure 1C), 96% ± 3.2% of the cells had excised *CEN4** after 180 min of estradiol treatment (Figures S1A–S1C). To monitor the effect of *CEN4** excision on condensation, chr IV contained the TetO array at the *TRP1* locus, bound by TetR-mCherry as above, and an array of 256 LacO sequences at the *LYS4* locus, labeled with LacI-GFP, 470 kb down the same chromosome arm. We then measured the physical distance separating these two loci in G1 (no contraction) and late anaphase cells (maximal contraction) (Neurohr et al., 2011; Vas et al., 2007), prior and after *CEN4** excision (noted *CEN4** and *cen4−*, respectively). Late anaphase cells were identified by a large bud and elongated mitotic spindle (labeled with CFP-tubulin) (Figure 1C). In parallel, quenching of the mCherry and GFP foci reported on chromatin compaction at these loci, as above. In these assays, *CEN4** chr IV properly contracted along its axis and compacted chromatin at both reporter loci in late anaphase, as evidenced by a drop in inter-loci distance and fluorescence intensity compared to G1 phase cells (Figures 1D and 1E) (Kruitwagen et al., 2015; Neurohr et al., 2011). In early anaphase, the concomitant action of the spindle, which pulls sister chromatids apart, and uncleaved cohesin rings puts chromosome arms under tension and stretches them (Straight et al., 1997; Renshaw et al., 2010). This is resolved in mid-anaphase when all cohesin is removed. Accordingly, contraction of the *CEN+* chr IV reached its maximum in late anaphase, i.e., in wild-type (WT) cells with an 8-μm-long spindle or in cells arrested at this stage using the *cdc15-1* temperature sensitive mutation (Hartwell et al., 1973) (Figures 1E, 1F, and S2A). Strikingly, wild-type cells barely condensed the chromosome during the course of unperturbed metaphases, which overlap with S phase in budding yeast (Kitamura et al., 2007) (Figure 1E). As expected (Neurohr et al., 2011; Kruitwagen et al., 2015), contraction and compaction of *CEN4** chr IV depended on Aurora B kinase, since they were abolished at 37°C in *ipl1-321* mutant cells, which express a temperature-sensitive mutant form of this protein (Figures 1E and S2B). Together, these data indicated that flanking *CEN4** with lox recombination sites or expression of Cre-EBD did not affect contraction and compaction of chr IV during mitosis. Thus, we next investigated the effect of *CEN4** excision on chr IV condensation upon estradiol treatment.

Two hours after estradiol addition, nearly 90% of the anaphase cells retained both copies of chr IV in the mother cell (Figures 1C, S3A, and S3B), consistent with *CEN4** being excised. Also, separation of chr IV chromatids was inefficient. In more than 80% of cells at least one of the labeled loci remained unsplit at the resolution of light microscopy (Figures 1C and S3B). We used these cells to unambiguously measure inter-focus distances. Fluorescence quenching was analyzed on split loci (Figure S3C). Strikingly, upon *CEN4** excision both the fluorescence intensity of the reporter dots (Figure 1D) and the distance between them (Figure 1E) failed to drop in anaphase compared to G1 phase cells. Though these chromosomes were not pulled and hence not stretched by the spindle as wild-type chromosomes, the physical distance between the labeled *TRP1* and *LYS4* loci remained significantly longer in *cen4−* than in wild-type anaphase cells. Thus, both chromatin compaction and arm contraction were abolished on the *cen−* chr IV. These effects closely resembled that of ablating the presumed catalytic activity of the deacetylase Hst2, a master regulator of condensation (Wilkins et al., 2014; Zhao et al., 2003; Kruitwagen et al., 2015) (Figures S3D and S3E). They were not due to a defect in anaphase progression, since *CEN4** and *cen4−* cells showed the same distributions of spindle length (Figure S4). They were specifically caused by excision of *CEN4**, because removal of another piece of chr IV did not alter chromosome condensation (see Figures S5A–S5C). Furthermore, arresting the *cen4−* mutant cells in late anaphase using the *cdc15-1* mutation did not restore the condensation of chr IV (Figures 1E and S2B). We conclude that *CEN4** is required for the mitotic condensation of at least chr IV during anaphase.

Averages and SEM are shown in black; n > 45 cells from at least three independent clones or technical replicates (A, B, D, and E). The average value of each clone (black or white circles) or technical replicate (gray circles) is plotted. Kruskal-Wallis tests (A, B, D, and E) were performed to test significance. ***p < 0.001, non-significance not shown. Scale bars, 2 μm.
See also Figures S1–S5.

Please cite this article in press as: Kruitwagen et al., Centromeres License the Mitotic Condensation of Yeast Chromosome Arms, Cell (2018), https://doi.org/10.1016/j.cell.2018.09.012

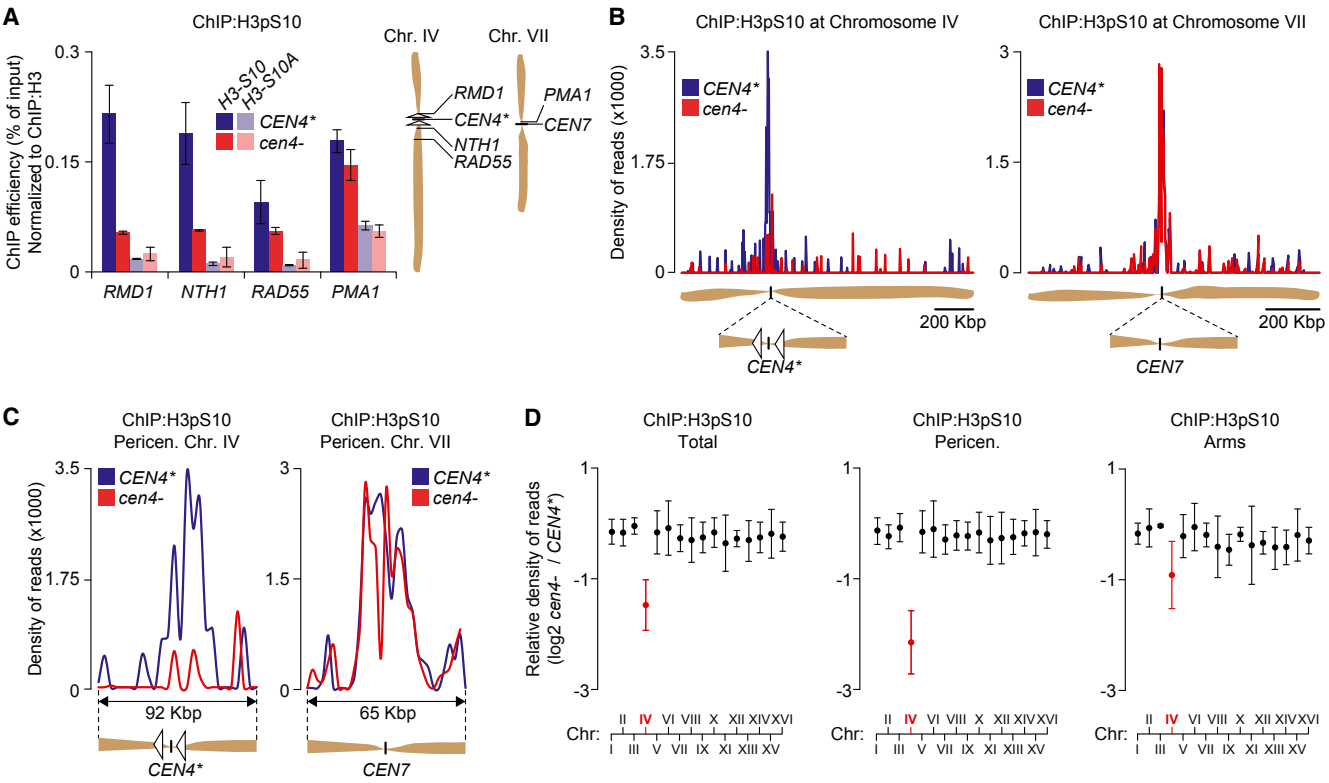

(legend on next page)

Centromeres Initiate Chromosome Condensation in *Cis*

Next, we wondered whether *CEN4** removal caused a defect in Aurora B activity, and, if it did, whether this defect was global or specific to chr IV. We probed Aurora B activity by looking at phosphorylation of serine 10 on histone H3 (H3-pS10) (Hsu et al., 2000) prior to and after *CEN4** excision, using chromatin immunoprecipitation (ChIP), followed by qPCR on several loci on chr IV (*RMD1*, *NTH1*, and *RAD55*) and chr VII (*PMA1*). All loci were efficiently precipitated from wild-type cells with an anti-H3-pS10 antibody, but not from H3-S10A mutant cells, where H3-S10 cannot be phosphorylated, demonstrating method specificity (Figure 2A). Remarkably, H3-pS10 levels were higher at *RMD1*, *NTH1*, and *PMA1*, all adjacent to their centromeres, than at the *RAD55* locus, positioned 50 kb away from *CEN4** (Figure 2A). In addition, *CEN4** excision strongly reduced H3-pS10 at *RMD1* and *NTH1* (juxtaposing *CEN4**), but not at *PMA1* (juxtaposing *CEN7*). These data suggest that the centromere promotes H3-pS10 in *cis*.

Accordingly, using ChIP sequencing (ChIP-seq), we found that each chromosome in exponentially growing cells displayed a ~30 kb pericentromeric zone of abundant H3-pS10 (Figures 2B–2D), as reported (Castellano-Pozo et al., 2013). Surprisingly however, H3-pS10 levels were very low elsewhere. This was true for asynchronous cells, but also for cells arrested in late anaphase (using the *cdc15-1* allele), where condensation is maximal (Figures S6A and S6B). Pericentromeric H3-pS10 depended on Aurora B activity, since it disappeared in *ipl1-321* mutant cells grown at the restrictive temperature (Figures 2E and 2F). In these cells, H3-pS10 was unchanged or slightly increased on chromosome arms, suggesting that Aurora B activity is primarily concentrated around centromeres and controls little if any H3 phosphorylation on the arms. Strikingly, in the *cen4−* cells pericentromeric H3-pS10 was reduced to background levels on chr IV, but was unaffected on other chromosomes (Figures 2B–2D; see chr VII in Figure 2B as an example). Furthermore, *CEN4** excision had little effect on H3-pS10 levels on chromosome arms, including those of chr IV (Figure 2D). Thus, centromeres are indeed required in *cis* to activate Aurora B on the chromosome, in a chromosome-autonomous manner. However, in budding yeast this activity is restricted to pericentromeric chromatin.

These data suggested that centromeres only act in *cis* in chromosome condensation. To test this possibility, we constructed diploid cells, where only one copy of chr IV was fluorescently labeled. The loxable *CEN4** was then introduced on one of the two copies of chr IV, either in *cis* of the labels or in *trans*. When *CEN4** was excised in *cis*, contraction and compaction of the reporter chromosome were impaired, like in haploid cells (Figures 2G and 2H). However, excision of *CEN4** in *trans* had no effect on the mitotic contraction and compaction of the reporter chromosome, demonstrating that the centromere acts solely in *cis*. Note that the mean TetO-LacO distance was higher in these diploids compared to haploid cells, likely because of scaling of condensation with spindle length and nuclear volume (Neurohr et al., 2011). Together, these results are consistent with Aurora B acting on a single, small locus around the centromere, from where it induces condensation of the entire chromosome. This interpretation would explain why non-centromeric DNA fails to condense during mitosis.

The Inner Kinetochore, but Not Intranuclear Localization, Controls Chromosome Condensation

Next, we considered two models for how the centromere establishes Aurora B activity on a chromosome. In the spatial model, Aurora B forms a short-range activity gradient focused on the spindle pole or at the place where centromeres cluster, as suggested in mammalian cells (Wang et al., 2011). In this case, *CEN* inactivation detaches the chromosome from the spindle, away from the Aurora B gradient. In the structural model, the centromere directly recruits Aurora B, possibly via structures attached to it.

The spatial model predicts that the nuclear localization of the *cen−* chromosome modulates its condensation. Furthermore, detaching the chromosome from the spindle should impair condensation, even if keeping the centromere intact. Using the labeled loci as a proxy for chromosome localization, we investigated whether *cen−* chromosomes located close to the spindle pole were more contracted than were distal ones (Figures 3A and 3B). This was not the case (Figure 3C). Using the outer-kinetochore mutation *dam1-1*, which abrogates kinetochore-microtubule attachment, we then tested whether spindle attachment is required for chromosomes to condense. To bypass the metaphase arrest caused by Dam1 inactivation, we abrogated the spindle assembly checkpoint (SAC) using the *mad2Δ* mutation. Remarkably, although the *dam1-1 mad2Δ* double-mutant cells mis-segregated their chromosomes as they proceeded through anaphase

Figure 2. Centromeres Induce a Chromosome-Specific Pericentromeric Zone around H3-pS10

(A) H3-pS10 and $H3_{total}$ were detected by ChIP-qPCR in *CEN4** and *cen4−* cells expressing wild-type H3-S10 or H3-S10A at the depicted loci. H3-pS10 ChIP signal was normalized to $H3_{total}$ ChIP. Error bars, SEM of n = 3 experiments.

(B) H3-pS10 ChIP-seq profiles for indicated chromosomes and genotypes. H3-pS10 signal is normalized to $H3_{total}$.

(C) Same as (B), except zoomed-in on the indicated pericentromeric regions.

(D) Quantification of H3-pS10 count changes between *CEN4** and *cen4−* cells for each chromosome. H3-pS10 counts are normalized as above. Left: whole chromosomes; middle: pericentromeric regions; and right: chromosome arms. Error bars, SEM of n = 3 ChIP-seq experiments. In (B)–(D), the background noise is subtracted (see the STAR Methods).

(E) Profile of H3-pS10 by ChIP-seq in *IPL1* and *ipl1-321* cells used in (B). Inlets: pericentromeric regions.

(F) Quantification of the change of the H3-pS10 signal between *ipl1-321* mutant and WT cells on the indicated chromosomal regions for all 16 chromosomes. Red: chr IV.

(G) *TRP1-LYS4* distances in the depicted diploid strains.

(H) Fluorescence intensities of indicated loci in strains used in (G).

Graphs, circles, and statistical analysis are like those in Figure 1 (H and G).

See also Figure S6 and Tables S1 and S2.

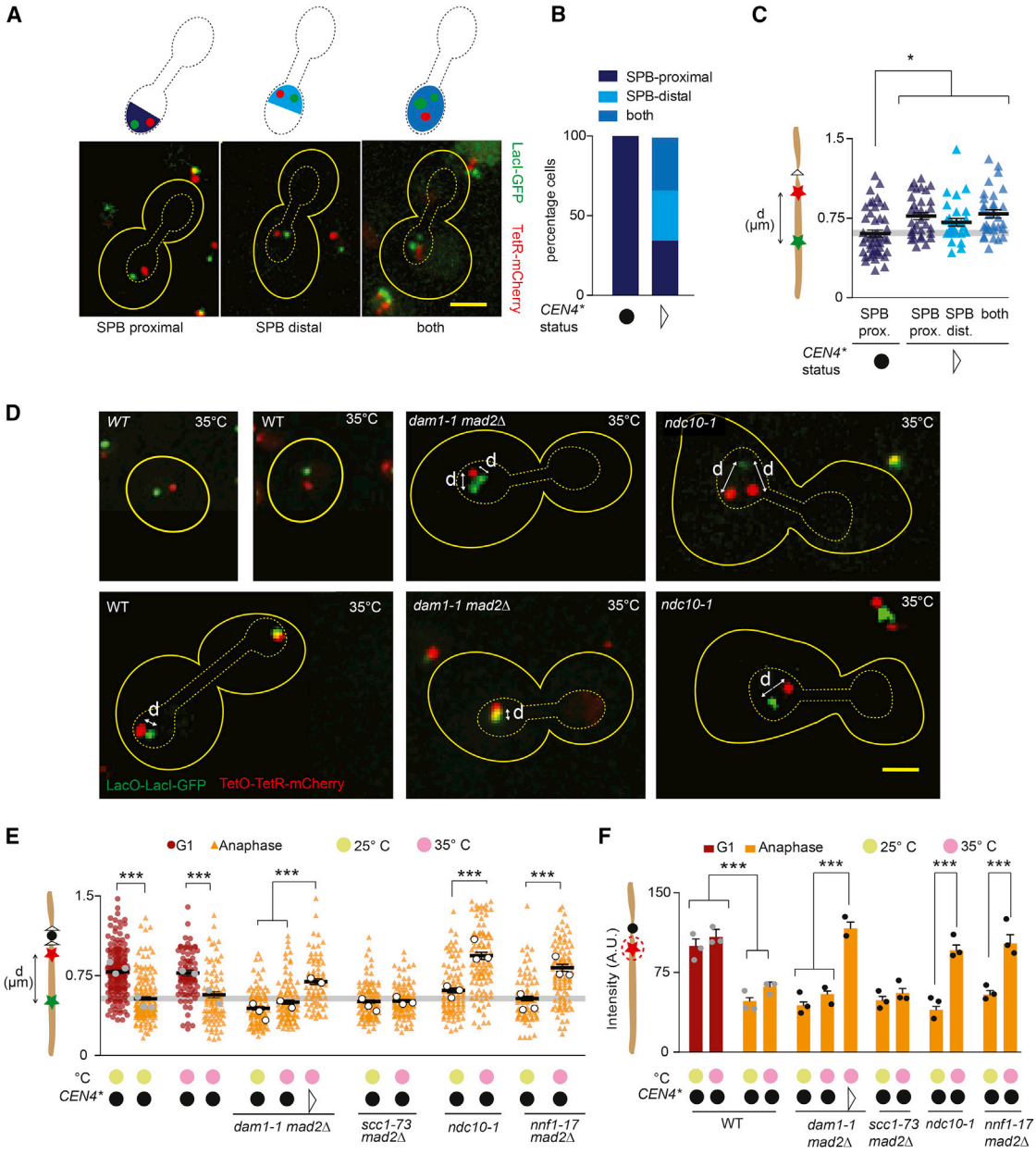

Figure 3. Centromere Functionally Promotes Chromosome Condensation

(A) Localization patterns for anaphase *cen4–* chromosomes.

(B) Distribution of cells of indicated *CEN4** status (like in Figure 1E) in the categories of (A).

(C) *TRP1-LYS4* distances for chr IV of indicated *CEN4** status at indicated positions in anaphase nuclei.

(D) Example WT G1 and anaphase cells of the indicated genotype grown at restrictive temperature. White arrows like in Figure 1C.

(E) *TRP1-LYS4* distance at indicated cell-cycle stages of indicated chromosomes in cells of indicated genotypes, grown at shown temperature.

(F) Fluorescence intensities of indicated foci in strains and conditions used in (E).

Thin, dashed line in (A) and (D) represents the outline of the nuclei. Scale bars, graphs, and statistics are like those in Figure 1.

(Figure 3D), they condensed chr IV properly (Figures 3E and 3F). Excision of *CEN4** in these cells again prevented chr IV condensation (Figures 3E and 3F). Since the *dam1-1 mad2Δ* double-mutant cells, *dam1-1 mad2Δ cen4–* triple-mutant cells, and the *cen4–* single-mutant cells all fail to attach chr IV to the spindle and localize it randomly in the nucleus, the contraction differences observed between these cells are not due to localization differences and biases in chromosome orientation in space. Thus, neither the proper attachment of the chromosomes to the spindle nor the chromosome's

localization near the spindle poles are prerequisites for condensation, refuting the spatial model. Rather, the effect of *CEN4** inactivation in these strains support the structural model.

Likewise, when the *scc1-73* mutant cells were grown at 37°C, abrogating cohesin function and sister chromatid cohesion (Marston, 2014; Stephens et al., 2011) they condensed chr IV properly in anaphase (Figures 3E and 3F). Thus, despite cohesin's role in chromosome condensation in metaphase-arrested cells (Guacci et al., 1997), it is not required for anaphase chromosome condensation.

Next, we tested whether the kinetochore still played any role in chromosome condensation. Inactivation of Nnf1 and Ndc10 disrupts most or the entire kinetochore, respectively (Biggins, 2013). Mutant cells carrying either the *ndc10-1* or the *nnf1-1* temperature sensitive alleles failed to condense chr IV at their restrictive temperature (Figures 3D–3F). Therefore, unlike the outer kinetochore and kinetochore-microtubule interaction, the yeast inner kinetochore fulfills an essential function in chromosome condensation.

The Centromere Acts Upstream of Aurora B, H3-pS10, and Hst2

Together, these data suggest that the centromere acts as a licensing locus for chromosome condensation: only DNA molecules carrying a centromere recruit Aurora B activity and condense in mitosis. To test whether Aurora B recruitment was required for chromosome condensation, we asked whether targeting Aurora B to a single locus on a *cen−* chromosome is sufficient to restore its condensation. We expressed Aurora B/Ipl1 as a TetR-fusion protein (Mendoza et al., 2009) and tested whether targeting it to the TetO array on chr IV bypassed *CEN4** function (Figure 4A). Remarkably, this construct fully restored both contraction (Figure 4B) and compaction of *cen−* chr IV (Figure 4C). Moreover, Ipl1-TetR promoted the condensation of both *CEN+* and *cen−* chr IV, regardless of the cell-cycle stage (Figures 4B and 4C). Targeting Ipl1-LacI to the LacO array further down the arm of chr IV had the same effect (Figures 4B and 4C). The kinase-dead mutant of Ipl1 (Ipl1-D227A) (Mendoza et al., 2009) failed to do so (Figure 4B). Also, expression of Ipl1-TetR in cells lacking a TetO array had no effect (Figure S7). Thus, recruitment of Aurora B activity onto a chromosome was sufficient to bypass the centromere's role in chromosome condensation. This effect depended neither on the locus nor on the DNA-binding domain to which Aurora B was fused. Consistent with these findings, the phospho-mimicking variant of H3, H3-S10D, also caused constitutive hyper-contraction and enhanced compaction of *CEN+* and *cen−* chr IV (Figures 4D and 4E). These effects depended on the deacetylase Hst2 (Figures 4D and 4E) (Kruitwagen et al., 2015; Wilkins et al., 2014). These data suggested that the role of the centromere in recruiting Aurora B is instrumental for its chromosome condensation function.

Targeting Ipl1 and H3-pS10 to DNA Circles Induces Their Compaction and Relaxes Their Retention

Our data indicated that non-centromeric DNA circles do not condense during mitosis because they are not licensed to do so. In fitting, expression of H3-S10D or targeting Ipl1-TetR to our model DNA circle (Figure 1A) triggered its compaction, in an Hst2-dependent manner (Figure 4F). Strikingly, whereas decompacted circles were efficiently retained in the mother cell, as previously reported (Denoth-Lippuner et al., 2014b; Shcheprova et al., 2008), forcing their compaction using either Ipl1-TetR or H3-S10D expression relaxed their confinement (Figure 4F), increasing their propagation frequency to that predicted for passively diffusing circles (Gehlen et al., 2011). Since H3-S10D was as efficient as Ipl1-TetR in this process, these effects are downstream of Aurora B and independent of its microtubule-related functions.

Thus, a consequence of the licensing of chromosome condensation by centromeres is that non-chromosomal DNA molecules do not condense, which is instrumental for their high-fidelity confinement into the mother cell during cell division.

Shugoshin Is Required for Chromosome Condensation

To better understand how Ipl1-TetR promoted chromosome condensation, we next characterized how its recruitment to a TetO array affected H3-pS10 on chr IV. As expected, H3-pS10 strongly increased at the array, independently of *CEN4** (Figures 5A and 5B). However, H3 phosphorylation remained unaffected anywhere else on chr IV (Figure 5C). Thus, Ipl1 promoted condensation of the entire chromosome from a single locus, in *cis*. This observation implies that effectors downstream of Aurora B must propagate the condensation signal along the chromosome.

To identify such factors, we tested whether other known kinetochore, centromere, and pericentromeric proteins, other than condensin, promote chromosome condensation in anaphase. Interestingly, cells lacking the SAC-gene *BUB1* failed to condense chr IV (Figures 5D and 5E). Since SAC inactivation by the *mad2Δ* mutation did not cause condensation defects (Figures 5D and 5E; see above), some non-SAC function of Bub1 was required for chromosome condensation. Importantly, one role of Bub1 is to mediate the recruitment of Shugoshin (Sgo1 in yeast) to pericentromeric chromatin. As such, Bub1 acts by phosphorylating histone H2A on S121 (H2A-pS121), creating a high-affinity binding-site for Sgo1. In metaphase cells, Sgo1 then promotes chromosome biorientation, tension sensing, cohesin protection, Aurora B activation, and condensin recruitment to centromeres by recruiting $PP2A^{Rts1}$ to chromatin (Marston, 2015). Consistent with cohesin being dispensable for anaphase condensation (see above), removal of the kinetochore proteins Ctf19 or Chl4, which promote the recruitment of cohesin around the centromere (Fernius and Marston, 2009; Hinshaw et al., 2017), did not affect chromosome condensation in anaphase (Figures 5D and 5E). Thus, Bub1 does not promote chromosome condensation by enforcing centromeric cohesion. However, like the *bub1Δ* mutation, inactivation of Sgo1 impaired both contraction and chromatin compaction of chr IV (Figures 5D and 5E). Consistent with Bub1 acting upstream of Sgo1, preventing phosphorylation of H2A-S121, and hence Sgo1 recruitment, also abrogated chromosome condensation (H2A-S121A) (Figures 5D and 5E). ChIP-seq analysis indicated that Shugoshin inactivation hardly affected the pattern of pS10 distribution along chromosomes

Please cite this article in press as: Kruitwagen et al., Centromeres License the Mitotic Condensation of Yeast Chromosome Arms, Cell (2018), https://doi.org/10.1016/j.cell.2018.09.012

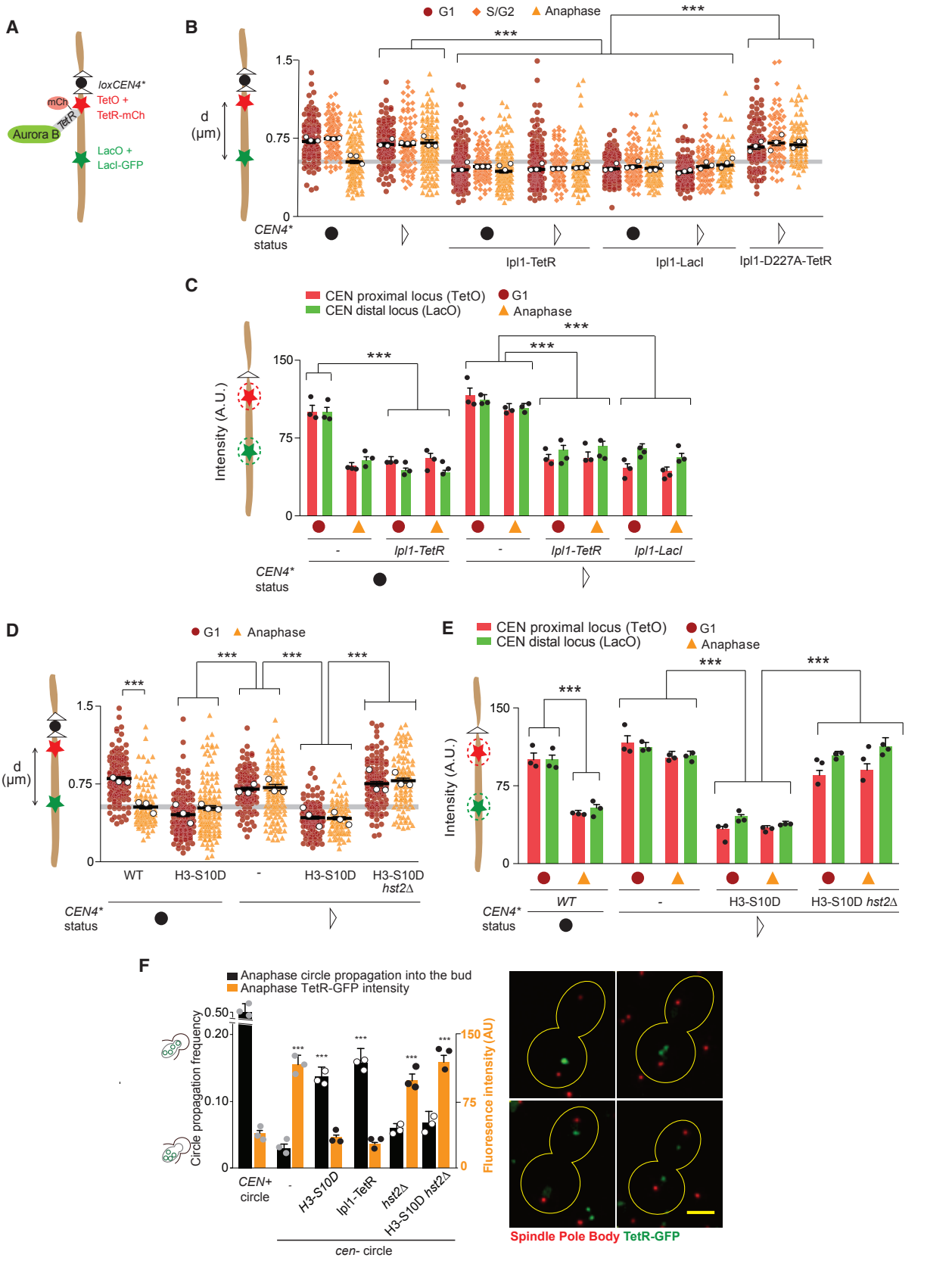

(legend on next page)

(Figures 5F and 5G), suggesting that Shugoshin acts downstream of Aurora B.

Since Shugoshin performs at least some of its functions by directly binding and recruiting the protein phosphatase $PP2A^{Rts1}$ to chromatin (Marston, 2015), we next tested whether PP2A also contributed to chromosome condensation. Strikingly, opposite of the *sgo1Δ* mutant, *rts1Δ* mutant cells, lacking the B' regulatory subunit of PP2A and interaction partner of Sgo1, constitutively condensed chr IV (Figures 5D, 5F, 5H, and 5I). Furthermore, this effect depended on Sgo1 function, but not on Bub1, indicating that the *rts1*Δ mutation derepressed a Bub1-independent function of Sgo1 in condensation. Accordingly, cells endogenously expressing the *sgo1-3A* mutant protein (Xu et al., 2009), which fails to interact with $PP2A^{Rts1}$, showed the same phenotype as the *rts1Δ* mutant cells (Figures 5H and 5I). Thus, Shugoshin acts in chromosome condensation independently of $PP2A^{Rts1}$. Instead, $PP2A^{Rts1}$ inhibited Sgo1 function in condensation. Strikingly, de-repressed Sgo1 no longer required Bub1 to promote condensation (Figures 5H and 5I).

The independence of Shugoshin on Bub1 function in the absence of Rts1 suggested that de-repressed Shugoshin might no longer require a centromere to promote chromosome condensation. Accordingly, our reporter *cen−* DNA circle underwent compaction in the *rts1Δ* and the *sgo1-3A* single-mutant cells (Figure 5J), as it did in the *H3-S10D* mutant cells (Figure 4F). In the *rts1Δ* and *H3-S10D* mutant cells, circle compaction was abrogated upon Sgo1 inactivation (Figure 5J). Furthermore, in the *rts1Δ* and *sgo1-3A* mutant cells, circle compaction did not rely on Bub1 function, demonstrating that when unleashed, Sgo1 acted on chromatin independently of the recruitment mechanisms active on metaphase chromosomes. In these situations, Sgo1 acted upstream or together with Hst2, since the *sgo1-3A hst2Δ* double-mutant cells failed to compact the circle. Finally, when circles were condensed, they were no longer-retained with high fidelity in the mother cell: in the *rts1Δ*, *sgo1-3A*, *rts1Δ bub1Δ*, and *sgo1-3A bub1Δ* single- and double-mutant cells, circle propagation to the bud reached the rate expected by random diffusion (12%–15%, Gehlen et al., 2011). Furthermore, preventing circle compaction in any of these cells by removing either Sgo1 or Hst2 restored their retention in the mother cell (Figure 5J). Thus, the chromatin compaction pathway releases chromatin from high-fidelity retention in the mother cell and relies on centromeres and the repression of Shugoshin by PP2A for being restricted to bona fide chromosomes.

Shugoshin Acts Downstream of Aurora B and H3-pS10

Next, we investigated the relationship between Shugoshin, Bub1 and Aurora B in more detail. As observed with Ipl1, tethering Sgo1 to the reporter chromosome in the *CEN4** and the *cen4−* cells, by fusing it to either TetR or LacI, promoted the constitutive condensation of the reporter chromosome (Figures 6A, 6B, and S7), and bypassed the requirement for a centromere, Bub1 and Aurora B (Figures 6A–6C). In contrast, Ipl1-TetR depended on Sgo1 function to promote chr IV contraction (Figure 6C). Accordingly, removal of Sgo1 abrogated the constitutive hyper-condensation phenotype of the *H3-S10D* mutant cells (Figure 6D). Furthermore, Sgo1-TetR expression did not restore H3-pS10 anywhere on the *cen4−* chromosome, as measured by ChIP-seq (Figures 6E and 6F). Thus, in wild-type cells Sgo1 acts downstream of Bub1 and Aurora B in chromosome condensation.

Sgo1 and Hst2 Are Required for the Condensation Signal to Propagate Downstream of Ipl1

Our data are consistent with a model in which centromeres license DNA condensation by gating the activation of Aurora B and Bub1, which acted upstream of Shugoshin. Downstream of Aurora activity, the condensation signal somehow propagates from the centromere to the entire chromosome. Thus, we wondered whether Sgo1 could promote signal propagation. To test this possibility, we developed the following assay (Figure 7A). Since Ipl1-TetR induces chr IV contraction and the compaction of both the TetO and LacO arrays (Figures 4A, 4B, and 7B), the signal elicited at the TetO array (called "the emitter" here) is propagated along the chromosome to the LacO array (used here as a receptor) (Figure 7A). Thus, inactivation of proteins involved in signal propagation should not affect chromatin compaction at the emitter upon Ipl1 binding but should prevent the receptor locus from compacting (Figure 7A). In contrast, a factor directly required for chromatin compaction should affect this process at both loci. Strikingly, inactivation of either Sgo1 or Hst2 did not affect chromatin compaction at the emitter but abrogated it at the receptor locus (Figures 7C and 7D). We conclude that both Hst2 and Shugoshin contribute to signal propagation downstream of Aurora B.

Consistently, Sgo1-TetR promoted the compaction of both the emitter and receptor arrays, even in cells expressing non-phosphorylatable H3-S10A (Figure 7D). In cells lacking Hst2, Sgo1-TetR only promoted compaction of the emitter, but not of the receptor. Thus, Hst2 promotes the propagation of the condensation signal downstream of Aurora B and Sgo1.

DISCUSSION

Control of Chromosome Condensation by a Non-diffusible Signal

In eukaryotes, activation of Cdk1 controls mitotic entry by spreading over the cell (Enserink and Kolodner, 2010). Therefore,

Figure 4. The Centromere Acts Upstream of Ipl1-H3pS10-Hst2 to Promote Condensation and Relaxes DNA Circle Retention

(A) Scheme of the experimental strategy.

(B and C) Contraction (B) and compaction (C) data from Figures 1E and 1D shown for reference and in cells expressing the indicated fusion proteins.

(D and E) Contraction (D) and compaction (E) as above. Data from Figures 1E and 1D are shown for reference.

(F) Fluorescence intensities (right scale) and rates of propagation to the daughter cells (left scale) of TetO-TetR-GFP-labeled DNA molecules indicated in cells of indicated genotype. Example cells containing GFP-marked DNA circle(s) and CFP-marked spindle pole bodies (SPBs) in late anaphase are shown.

Scale bar, graphs, circles, and statistics are like those in Figure 1, except for the propagation rates in (F), where the SD is shown.

See also Figure S7.

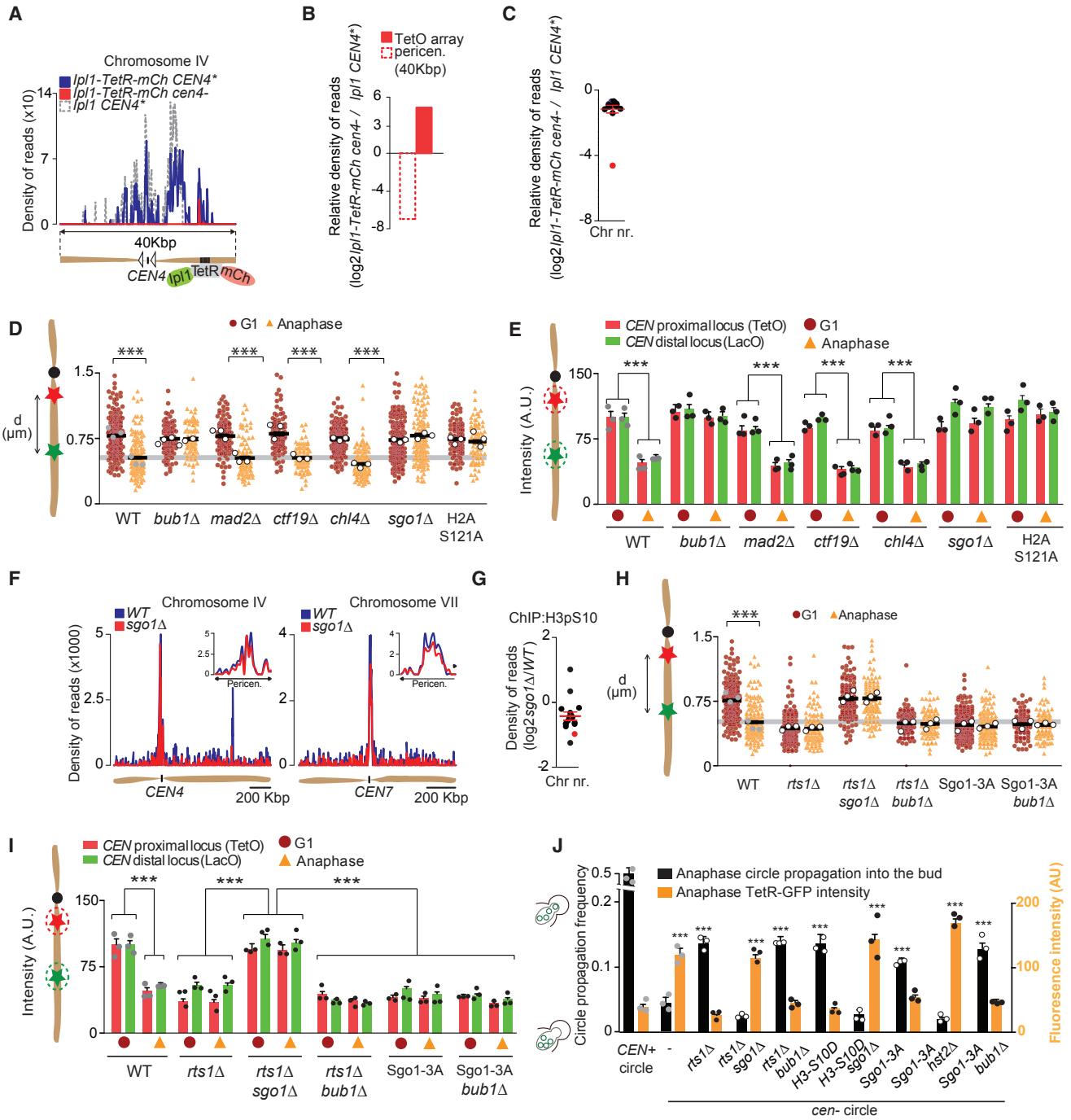

Figure 5. Shugoshin Promotes Chromosome Condensation

(A) Profile of H3-pS10 levels used in Figure 2C at the pericentromere of chr IV in cells of the indicated genotypes. The displayed region is centered on *CEN4** and contains the TetO array (see scheme below the graph). The signal was normalized like in Figure 2C.

(B) Quantification of the signals in (A) for the whole 40-kb pericentromeric and TetO array regions. Normalization is like that in Figure 2C (see the STAR Methods).

(C) Changes of H3-pS10 levels between *CEN4** and *cen4−* cells expressing Ipl1-TetR-mCherry are shown for each of the 16 chromosomes. Red dot: chr IV. See the STAR Methods for normalization.

(D and E) Contraction (D) and compaction data (E) in cells of indicated cell-cycle stage and indicated genotype. WT contraction data from Figure 3E and 3F shown as reference.

(F) H3-pS10 levels on chr IV and VII in cells of the indicated genotype established and shown like in Figure 2E.

(legend continued on next page)

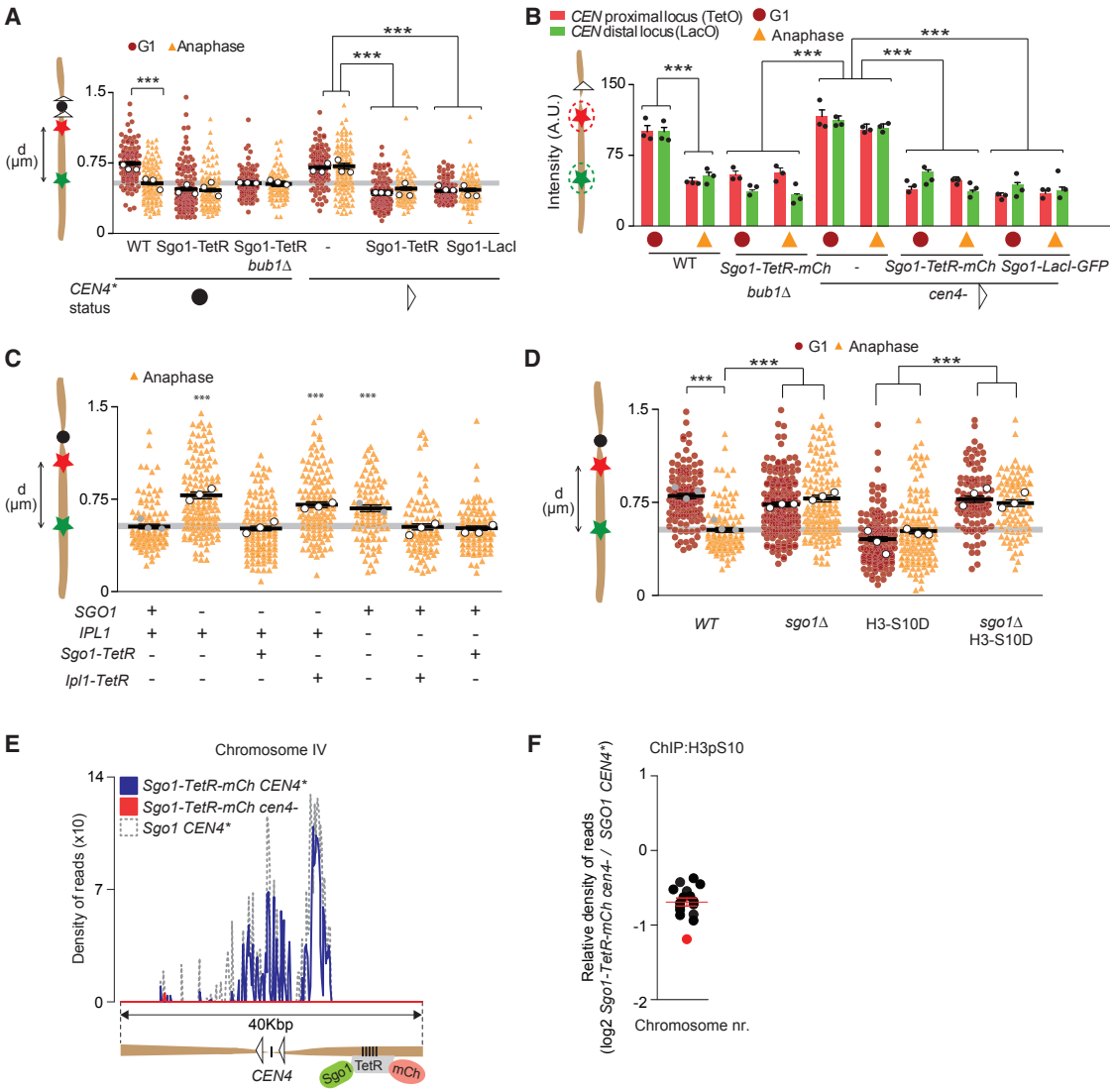

Figure 6. Shugoshin Acts Downstream of Aurora B

(A and B) Contraction (A) and compaction (B) data in cells in the indicated cell-cycle stage expressing the indicated fusion proteins. *CEN4** and *cen4−* data from Figures 1E and 1D are shown for reference.

(C) Contraction of chr IV in anaphase cells expressing the indicated fusion proteins and of indicated genotypes. For reference, the data for *ipl1-321*, WT, and *sgo1Δ*, mutant cells are repeated from Figures 1E, 4D, and 5D, respectively.

(D) Compaction data for cells of indicated genotype in indicated cell-cycle stage. WT, *H3S10D*, and *sgo1Δ* data from Figures 4D and 5D, respectively, are shown as reference. Graphs, circles, and statistics are like those in Figure 1

(E) Profile of H3-pS10 levels from Figure 5E for the indicated region of chr IV in cells from the indicated genotypes.

(F) Changes in H3-pS10 levels between *sgo1-TetR-mCh cen4−* cells and *SGO1 CEN4** cells on each chromosome. Red dot, chr IV; black, other chromosome. See also Figure S7.

it was tempting to assume that chromosome condensation was also induced globally. This work, however, argues that chromosome condensation in budding yeast is not solely driven by diffusion. Aurora B activity is restricted to the pericentromeric region of individual chromosomes and centromeres promote condensation of the chromosome arms strictly in *cis*. Chromosome condensation is therefore a chromosome-autonomous and chromosome-restricted process. Accordingly, our study

(G) Changes in H3-pS10 levels between cells of indicated genotypes on indicated chromosome regions. Each chromosome is shown. Red: chr IV, other chromosomes black. Normalization is like that in Figures 2D and 2F.

(H and I) Contraction (H) and compaction (I) data in cells in the indicated cell-cycle stage and of indicated genotype. WT contraction and compaction data from Figures 3E and 5E, respectively, shown as reference. Graphs, circles, and statistics are like those in Figure 1.

(J) Compaction and propagation of the indicated DNA circles in cells of the indicated genotype like in Figure 4F. WT from Figure 4F is shown for reference.

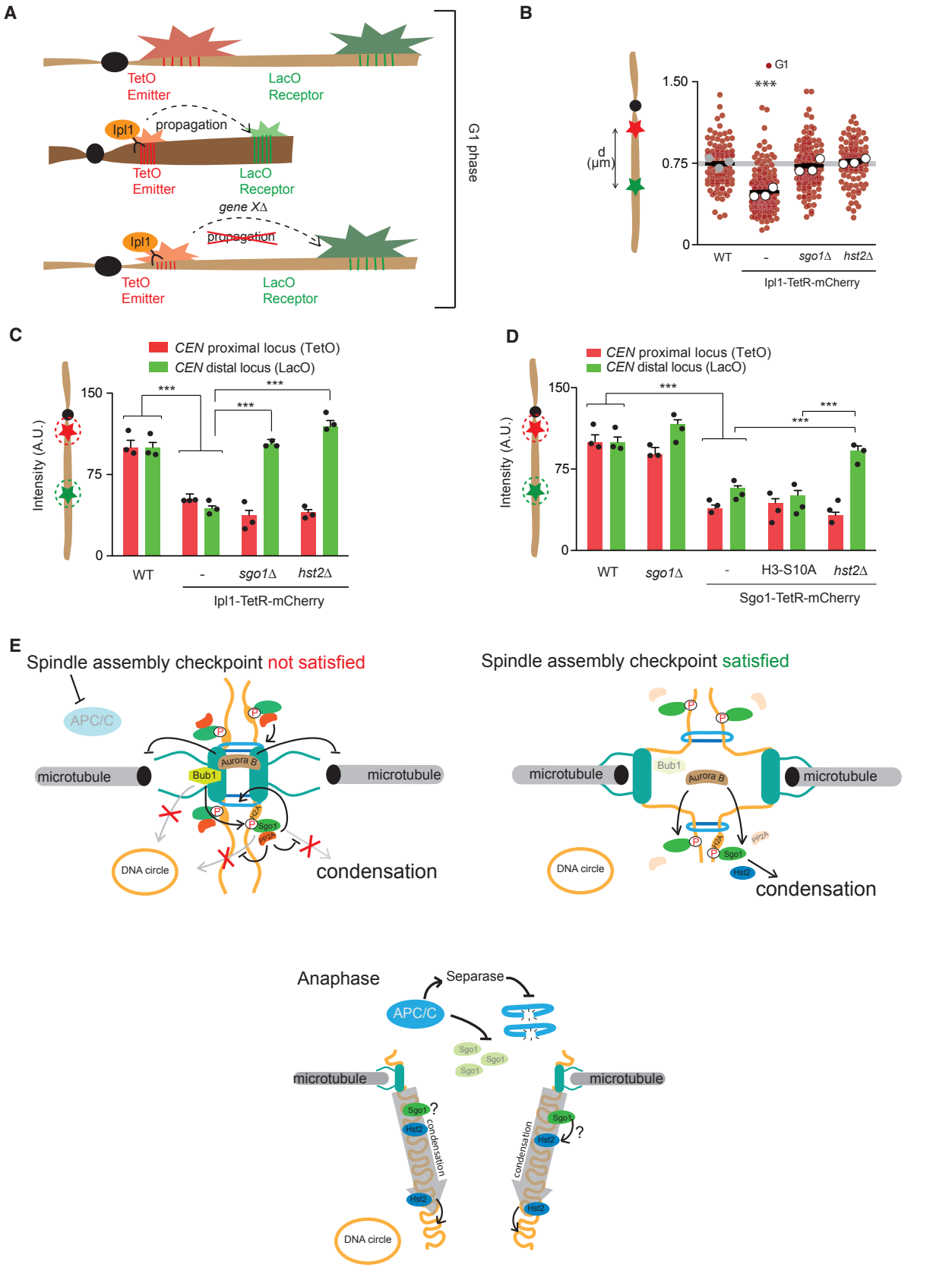

(legend on next page)

identifies three steps in the control of chromosome condensation (Figure 7E).

First, centromeres control the timing of condensation. We hypothesize that two upstream cell-cycle-dependent signals reach the centromere by diffusion: the Bub1-dependent recruitment of Sgo1-PP2A and the activity controlling Aurora B. However, their functions in condensation are inhibited, hypothetically by PP2A. We hypothesize that this inhibition is likely lifted upon SAC satisfaction. In fitting, in *rts1Δ* mutant cells, the cell cycle seems to lose its control on condensation, causing chromosomes to condense even in G1 phase.

Second, prior to anaphase, at the (peri)centromeric region, Aurora B sets up the condensation signal. It might do so through H3-pS10, since expression of H3-S10D elicits constitutive chromosome condensation (Kruitwagen et al., 2015; Wilkins et al., 2014). However, since H3-S10A mutant cells still contract their chromosome arms in an Hst2-dependent manner (Kruitwagen et al., 2015), this is not the sole mode of Aurora B function. A second route might involve the activation of Shugoshin. Indeed, our data place Aurora B upstream of Shugoshin, which carries consensus Aurora B phosphorylation sites.

Third, the signal spreads along the chromosome and triggers its condensation. This process must rely on proteins that are chromosome-bound and activated locally. We propose that Shugoshin and Hst2 promote condensation either by initiating the spreading of yet other downstream effectors along chromosomes (such as condensin) or by being part of the spreading module itself. We favor the second option for the following reasons. First, provided that a very small pool of Shugoshin remains somehow tethered to chromosomes after SAC satisfaction, its redistribution to chromosome arms could promote condensation. Although Shugoshin has not been observed on chromosome arms in mitosis (Eshleman and Morgan, 2014; Nerusheva et al., 2014; Marston, 2015), it localizes there in meiosis (Katis et al., 2004). Second, because Hst2 is directly deacetylating H4-K16, we propose that it is part of the traveling unit that propagates the signal (Wilkins et al., 2014). Since Aurora B activity and H3-pS10 do not propagate beyond pericentromeric chromatin in yeast, some other mechanism must recruit Hst2 to chromosomes arms, as suggested (Kruitwagen et al., 2015).

Together, this three-step mechanism ensures that chromosome condensation is tightly coordinated with cell-cycle progression and remains chromosome autonomous. Indeed, the coordination of chromatin organization by centromeres may help orchestrate two opposite and mutually exclusive roles of Shugoshin at centromeres and on chromosome arms, one depending on PP2A, whereas the other does not.

Centromere-Chromosome Relationships in Animal Cells

One of the first studies describing H3-pS10 pointed out that it takes place first at centromeres before reaching chromosome arms (Hendzel et al., 1997). Similarly, condensin recruitment seems to start from centromeres (Oliveira et al., 2005). These observations underline possible similarities in how yeast and animal cells control chromosome condensation. However, unlike in budding yeast, H3-pS10 is not confined to centromeres in animals and there is no evidence that kinetochore inactivation affects chromosome condensation. Therefore, other elements of these more complex centromeres might have taken over the control of chromosome condensation.

More generally, our work provides another example of a single locus controlling the organization of an entire chromosome or large domains thereof, as described for X chromosome inactivation in mammals (Cerase et al., 2015) and the Hox genes in vertebrates (Montavon and Duboule, 2013). Therefore, the role of centromeres in chromosome condensation emerges as a possibly powerful system for dissecting the control of chromosome dynamics beyond mitosis.

Condensation as a Distinctive Feature of Chromosomal versus Non-chromosomal Chromatin

Beyond its actual genome enclosed in its chromosomes, the nucleus of eukaryotic cells is occasionally confronted with the intrusion of other DNA molecules. These include exogenous molecules, such as viral genomes (Jern and Coffin, 2008), and molecules of endogenous origin, such as DNA circles (Cohen and Segal, 2009; Kuttler and Mai, 2007; Møller et al., 2015, 2018) and mobilized transposable elements (Beauregard et al., 2008). Most of these can have adverse effects on the cell or the organism, either because they hijack the cellular machinery, such as viruses, or by producing genetic noise. For example, in many cancers extra-chromosomal double minutes amplify proto-oncogenes, drive tumorigenesis (Fan et al., 2011; Von Hoff et al., 1988; Turner et al., 2017), and contribute to drug resistance (Kuttler and Mai, 2007). In budding yeast, the accumulation of DNA circles in the mother cell through asymmetric segregation is a major determinant of replicative aging (reviewed in Denoth-Lippuner et al., 2014a). That yeast cells efficiently retain non-chromosomal DNA circle in the mother nucleus suggest that they can actively sort these circles away from chromosomal chromatin (Denoth-Lippuner et al., 2014b; Gehlen et al., 2011; Shcheprova et al., 2008; Ouellet and Barral 2012). The autonomy of chromosomes for condensation identified in this study provides a possible model for how yeast distinguishes non-chromosomal DNA from bona fide chromosomes.

Our observations suggest that yeast centromeres, in addition to their other well-described roles in chromosome attachment to the spindle, act as licenses for mitotic DNA propagation also by releasing chromatin from retention in the mother cell. Mechanistically, we hypothesize that retention could be due to the uncondensed state affecting the ability of circles to

Figure 7. Shugoshin Propagates a Signal to Promote Compaction of Chromosome Arms

(A) Scheme of the experimental strategy.

(B and C) Contraction (B) and compaction (C) data in G1 phase upon expressing Ipl1-TetR-mCherry in cells of the indicated genotypes. WT repeated from Figures 1E and 1D and Ipl1-TetR data repeated from Figures 4B and 4C for reference.

(D) Compaction data in G1 cells upon expressing Sgo1-TetR-mCherry in cells of indicated genotypes. Statistics and circles are like those in Figure 1.

(E) Model (see main text).

pass through the bud neck, or uncondensed chromatin might somehow fail to detach from the nuclear envelope during mitosis (Shcheprova et al., 2008; Denoth-Lippuner et al., 2014b). Thereby, we suggest that centromeres assume the role of identity determinants, specifying chromosomes as part of the genome. This conception of the centromere makes several predictions.

First, it suggests that centromeres play a so-far underexplored role in immunity mechanisms, protecting the cell and its progeny from the propagation and interference of infectious genetic material. In animal cells, recombinant DNA injected in the nucleus is soon expelled from the nucleus through an uncharacterized budding mechanism (Shimizu et al., 2005). Strikingly, recent data demonstrated that centromeric satellite DNA promotes the retention of fly chromosomes in interphase nuclei, supporting the idea that centromeres act as self-determinants in insects (Jagannathan et al., 2018). It would be interesting to test whether centromere- and condensation-related functions help cells identify and eliminate non-self DNA more broadly.

Second, if centromeres are indeed self-determinants they could be part of an evolutionary arms race with pathogens. This might explain why centromeres and many kinetochore proteins evolve rapidly, even though they are so crucial for an organism's proliferation, development, and survival (Henikoff et al., 2001).

Third, if centromeres were to act as identity determinants they could cause genetic conflicts in hybrids, which has also been observed (Maheshwari and Barbash, 2011). As such, the role assigned to centromeres and centromeric factors in meiotic drive might directly relate to the function that we propose they play in genomic immunity, i.e., in deciding which DNA molecules pass to the next generation.

STAR★METHODS

Detailed methods are provided in the online version of this paper and include the following:

- KEY RESOURCES TABLE
- CONTACT FOR REAGENT AND RESOURCE SHARING
- EXPERIMENTAL MODEL AND SUBJECT DETAILS
  - Strains and media
- METHOD DETAILS
  - CRISPR/Cas9 mediated introduction of point mutations
  - Alpha-factor-mediated G1 arrest
  - CEN4* excision
  - CEN4* excision efficiency assay
  - Construction and excision of lox:mCherry:NatMX:lox:GFP
  - Microscopy
  - DNA circle propagation assay
  - ChIP-seq and ChIP-qPCR experiments
- QUANTIFICATION AND STATISTICAL ANALYSIS
  - DNA compaction and contraction analysis
  - Statistics for microscopy experiments
  - DNA circle propagation frequency calculations
  - Analysis of ChIP sequencing data
- DATA AND SOFTWARE AVAILABILITY

SUPPLEMENTAL INFORMATION

Supplemental Information includes seven figures and three tables and can be found with this article online at https://doi.org/10.1016/j.cell.2018.09.012.

ACKNOWLEDGMENTS

The authors express their gratitude to the members of the Barral and Kroschewski laboratories; Karsten Weis, Ulrike Kutay, and Heinz Neumann; and anonymous reviewers for insightful inputs. P.C. acknowledges Ignacio Garcia for assistance with data analysis. This project was supported by a BarrAge grant from the European Research Council and a grant from ETH (to Y.B.), the Norwegian Research Council (221694 to J.E.; 221920 to P.C.), Norwegian Cancer Society Project Numbers (144176 and 182524) (to J.E.), and Helse Sør Øst (2017065) (to P.C.). This work was partly supported by the Research Council of Norway through its Centers of Excellence funding scheme (project number 262652).

AUTHOR CONTRIBUTIONS

Conceptualization, Y.B.; Investigation, T.K., P.C., and A.D.-L.; Validation, T.K. and P.C.; Formal Analysis, Y.B., T.K., and P.C.; Data Curation, T.K. and P.C.; Visualization, T.K. and P.C.; Writing – Original Draft, Y.B. and T.K.; Writing – Review & Editing, Y.B., T.K., J.E., P.C., and A.D.-L.; Funding Acquisition, Y.B., J.E., and P.C.; Resources, Y.B., J.E., and P.C.; Supervision Y.B. and J.E.

DECLARATION OF INTERESTS

P.C. is a founder and member of the board of directors of Hemispherian AS. All other authors declare no competing interests.

Received: July 1, 2017
Revised: June 14, 2018
Accepted: September 7, 2018
Published: October 11, 2018

REFERENCES

Antonin, W., and Neumann, H. (2016). Chromosome condensation and decondensation during mitosis. Curr. Opin. Cell Biol. *40*, 15–22.

Beauregard, A., Curcio, M.J., and Belfort, M. (2008). The take and give between retrotransposable elements and their hosts. Annu. Rev. Genet. *42*, 587–617.

Biggins, S. (2013). The composition, functions, and regulation of the budding yeast kinetochore. Genetics *194*, 817–846.

Castellano-Pozo, M., Santos-Pereira, J.M., Rondón, A.G., Barroso, S., Andújar, E., Pérez-Alegre, M., García-Muse, T., and Aguilera, A. (2013). R loops are linked to histone H3 S10 phosphorylation and chromatin condensation. Mol. Cell *52*, 583–590.

Cerase, A., Pintacuda, G., Tattermusch, A., and Avner, P. (2015). Xist localization and function: new insights from multiple levels. Genome Biol. *16*, 166.

Chymkowitch, P., Eldholm, V., Lorenz, S., Zimmermann, C., Lindvall, J.M., Bjørås, M., Meza-Zepeda, L.A., and Enserink, J.M. (2012). Cdc28 kinase activity regulates the basal transcription machinery at a subset of genes. Proc. Natl. Acad. Sci. USA *109*, 10450–10455.

Chymkowitch, P., Nguéa, A.P., Aanes, H., Koehler, C.J., Thiede, B., Lorenz, S., Meza-Zepeda, L.A., Klungland, A., and Enserink, J.M. (2015). Sumoylation of Rap1 mediates the recruitment of TFIID to promote transcription of ribosomal protein genes. Genome Res. *25*, 897–906.

Chymkowitch, P., Nguéa P, A., Aanes, H., Robertson, J., Klungland, A., and Enserink, J.M. (2017). TORC1-dependent sumoylation of Rpc82 promotes RNA polymerase III assembly and activity. Proc. Natl. Acad. Sci. USA *114*, 1039–1044.

Cohen, S., and Segal, D. (2009). Extrachromosomal circular DNA in eukaryotes: possible involvement in the plasticity of tandem repeats. Cytogenet. Genome Res. *124*, 327–338.

Dai, J., Hyland, E.M., Yuan, D.S., Huang, H., Bader, J.S., and Boeke, J.D. (2008). Probing nucleosome function: a highly versatile library of synthetic histone H3 and H4 mutants. Cell *134*, 1066–1078.

Denoth-Lippuner, A., Julou, T., and Barral, Y. (2014a). Budding yeast as a model organism to study the effects of age. FEMS Microbiol. Rev. *38*, 300–325.

Denoth-Lippuner, A., Krzyzanowski, M.K., Stober, C., and Barral, Y. (2014b). Role of SAGA in the asymmetric segregation of DNA circles during yeast ageing. eLife *3*.. https://doi.org/10.7554/eLife.03790.

Enserink, J.M., and Kolodner, R.D. (2010). An overview of Cdk1-controlled targets and processes. Cell Div. *5*, 11.

Eshleman, H.D., and Morgan, D.O. (2014). Sgo1 recruits PP2A to chromosomes to ensure sister chromatid bi-orientation during mitosis. J. Cell Sci. *127*, 4974–4983.

Fan, Y., Mao, R., Lv, H., Xu, J., Yan, L., Liu, Y., Shi, M., Ji, G., Yu, Y., Bai, J., et al. (2011). Frequency of double minute chromosomes and combined cytogenetic abnormalities and their characteristics. J. Appl. Genet. *52*, 53–59.

Fernius, J., and Marston, A.L. (2009). Establishment of cohesion at the pericentromere by the Ctf19 kinetochore subcomplex and the replication fork-associated factor, Csm3. PLoS Genet. *5*, e1000629.

Gehlen, L.R., Nagai, S., Shimada, K., Meister, P., Taddei, A., and Gasser, S.M. (2011). Nuclear geometry and rapid mitosis ensure asymmetric episome segregation in yeast. Curr. Biol. *21*, 25–33.

Guacci, V., Koshland, D., and Strunnikov, A. (1997). A direct link between sister chromatid cohesion and chromosome condensation revealed through the analysis of MCD1 in S. cerevisiae. Cell *91*, 47–57.

Hartwell, L.H., Mortimer, R.K., Culotti, J., and Culotti, M. (1973). Genetic control of the cell division cycle in yeast: v. genetic analysis of cdc mutants. Genetics *74*, 267–286.

Hendzel, M.J., Wei, Y., Mancini, M.A., Van Hooser, A., Ranalli, T., Brinkley, B.R., Bazett-Jones, D.P., and Allis, C.D. (1997). Mitosis-specific phosphorylation of histone H3 initiates primarily within pericentromeric heterochromatin during G2 and spreads in an ordered fashion coincident with mitotic chromosome condensation. Chromosoma *106*, 348–360.

Henikoff, S., Ahmad, K., and Malik, H.S. (2001). The centromere paradox: stable inheritance with rapidly evolving DNA. Science *293*, 1098–1102.

Hinshaw, S.M., Makrantoni, V., Harrison, S.C., and Marston, A.L. (2017). The kinetochore receptor for the cohesin loading complex. Cell *171*, 72–84.e13.

Hsu, J.Y., Sun, Z.W., Li, X., Reuben, M., Tatchell, K., Bishop, D.K., Grushcow, J.M., Brame, C.J., Caldwell, J.A., Hunt, D.F., et al. (2000). Mitotic phosphorylation of histone H3 is governed by Ipl1/aurora kinase and Glc7/PP1 phosphatase in budding yeast and nematodes. Cell *102*, 279–291.

Jagannathan, M., Cummings, R., and Yamashita, Y.M. (2018). A conserved function for pericentromeric satellite DNA. eLife Sciences *7*, e34122.

Janke, C., Magiera, M.M., Rathfelder, N., Taxis, C., Reber, S., Maekawa, H., Moreno-Borchart, A., Doenges, G., Schwob, E., Schiebel, E., and Knop, M. (2004). A versatile toolbox for PCR-based tagging of yeast genes: new fluorescent proteins, more markers and promoter substitution cassettes. Yeast *21*, 947–962.

Jern, P., and Coffin, J.M. (2008). Effects of retroviruses on host genome function. Annu. Rev. Genet. *42*, 709–732.

Katis, V.L., Galova, M., Rabitsch, K.P., Gregan, J., and Nasmyth, K. (2004). Maintenance of cohesin at centromeres after meiosis I in budding yeast requires a kinetochore-associated protein related to MEI-S332. Curr. Biol. *14*, 560–572.

Kitamura, E., Tanaka, K., Kitamura, Y., and Tanaka, T.U. (2007). Kinetochore microtubule interaction during S phase in Saccharomyces cerevisiae. Genes Dev. *21*, 3319–3330.

Kruitwagen, T., Denoth-Lippuner, A., Wilkins, B.J., Neumann, H., and Barral, Y. (2015). Axial contraction and short-range compaction of chromatin synergistically promote mitotic chromosome condensation. eLife *4*, e1039.

Kschonsak, M., and Haering, C.H. (2015). Shaping mitotic chromosomes: From classical concepts to molecular mechanisms. BioEssays *37*, 755–766.

Kuttler, F., and Mai, S. (2007). Formation of non-random extrachromosomal elements during development, differentiation and oncogenesis. Semin. Cancer Biol. *17*, 56–64.

Langmead, B., and Salzberg, S.L. (2012). Fast gapper-read alignment with Bowtie 2. Nature Methods *9*, 357–359.

Laughery, M.F., Hunter, T., Brown, A., Hoopes, J., Ostbye, T., Shumaker, T., and Wyrick, J.J. (2015). New vectors for simple and streamlined CRISPR-Cas9 genome editing in Saccharomyces cerevisiae. Yeast *32*, 711–720.

Lengefeld, J., Hotz, M., Rollins, M., Baetz, K., and Barral, Y. (2017). Budding yeast Wee1 distinguishes spindle pole bodies to guide their pattern of age-dependent segregation. Nat. Cell Biol. *19*, 941–951.

Lindstrom, D.L., and Gottschling, D.E. (2009). The mother enrichment program: a genetic system for facile replicative life span analysis in Saccharomyces cerevisiae. Genetics *183*, 413–422, 1SI-13SI.

Longtine, M.S., McKenzie, A., 3rd, Demarini, D.J., Shah, N.G., Wach, A., Brachat, A., Philippsen, P., and Pringle, J.R. (1998). Additional modules for versatile and economical PCR-based gene deletion and modification in Saccharomyces cerevisiae. Yeast *14*, 953–961.

Maheshwari, S., and Barbash, D.A. (2011). The genetics of hybrid incompatibilities. Annu. Rev. Genet. *45*, 331–355.

Marston, A.L. (2014). Chromosome segregation in budding yeast: sister chromatid cohesion and related mechanisms. Genetics *196*, 31–63.

Marston, A.L. (2015). Shugoshins: tension-sensitive pericentromeric adaptors safeguarding chromosome segregation. Mol. Cell. Biol. *35*, 634–648.

Megee, P.C., and Koshland, D. (1999). A functional assay for centromere-associated sister chromatid cohesion. Science *285*, 254–257.

Mendoza, M., Norden, C., Durrer, K., Rauter, H., Uhlmann, F., and Barral, Y. (2009). A mechanism for chromosome segregation sensing by the NoCut checkpoint. Nat. Cell Biol. *11*, 477–483.

Møller, H.D., Parsons, L., Jørgensen, T.S., Botstein, D., and Regenberg, B. (2015). Extrachromosomal circular DNA is common in yeast. Proc. Natl. Acad. Sci. USA *112*, E3114–E3122.

Møller, H.D., Mohiyuddin, M., Prada-Luengo, I., Sailani, M.R., Halling, J.F., Plomgaard, P., Maretty, L., Hansen, A.J., Snyder, M.P., Pilegaard, H., et al. (2018). Circular DNA elements of chromosomal origin are common in healthy human somatic tissue. Nat. Commun. *9*, 1069.

Montavon, T., and Duboule, D. (2013). Chromatin organization and global regulation of Hox gene clusters. Philos. Trans. R. Soc. Lond. B Biol. Sci. *368*, 20120367.

Nerusheva, O.O., Galander, S., Fernius, J., Kelly, D., and Marston, A.L. (2014). Tension-dependent removal of pericentromeric shugoshin is an indicator of sister chromosome biorientation. Genes Dev. *28*, 1291–1309.

Neurohr, G., Naegeli, A., Titos, I., Theler, D., Greber, B., Díez, J., Gabaldón, T., Mendoza, M., and Barral, Y. (2011). A midzone-based ruler adjusts chromosome compaction to anaphase spindle length. Science *332*, 465–468.

Oliveira, R.A., Coelho, P.A., and Sunkel, C.E. (2005). The condensin I subunit Barren/CAP-H is essential for the structural integrity of centromeric heterochromatin during mitosis. Mol. Cell. Biol. *25*, 8971–8984.

Ouellet, J., and Barral, Y. (2012). Organelle segregation during mitosis: lessons from asymmetrically dividing cells. J. Cell Biol. *196*, 305–313.

Piskadlo, E., and Oliveira, R.A. (2016). Novel insights into mitotic chromosome condensation. F1000Res. *5*, 1807.

Quinlan, A.R., and Hall, I.M. (2010). BEDTools: a flexible suite of utilities for comparing genomic features. Bioinformatics *26*, 841–842.

Renshaw, M.J., Ward, J.J., Kanemaki, M., Natsume, K., Nédélec, F.J., and Tanaka, T.U. (2010). Condensins promote chromosome recoiling during

early anaphase to complete sister chromatid separation. Dev. Cell *19*, 232–244.

Rothbart, S.B., Dickson, B.M., Raab, J.R., Grzybowski, A.T., Krajewski, K., Guo, A.H., Shanle, E.K., Josefowicz, S.Z., Fuchs, S.M., Allis, C.D., et al. (2015). An interactive database for the assessment of histone antibody specificity. Mol. Cell *59*, 502–511.

Shcheprova, Z., Baldi, S., Frei, S.B., Gonnet, G., and Barral, Y. (2008). A mechanism for asymmetric segregation of age during yeast budding. Nature *454*, 728–734.

Shimizu, N., Kamezaki, F., and Shigematsu, S. (2005). Tracking of microinjected DNA in live cells reveals the intracellular behavior and elimination of extrachromosomal genetic material. Nucleic Acids Res. *33*, 6296–6307.

Stephens, A.D., Haase, J., Vicci, L., Taylor, R.M., 2nd, and Bloom, K. (2011). Cohesin, condensin, and the intramolecular centromere loop together generate the mitotic chromatin spring. J. Cell Biol. *193*, 1167–1180.

Straight, A.F., Marshall, W.F., Sedat, J.W., and Murray, A.W. (1997). Mitosis in living budding yeast: anaphase A but no metaphase plate. Science *277*, 574–578.

Turner, K.M., Deshpande, V., Beyter, D., Koga, T., Rusert, J., Lee, C., Li, B., Arden, K., Ren, B., Nathanson, D.A., et al. (2017). Extrachromosomal oncogene amplification drives tumour evolution and genetic heterogeneity. Nature *543*, 122–125.

Vas, A.C.J., Andrews, C.A., Kirkland Matesky, K., and Clarke, D.J. (2007). In vivo analysis of chromosome condensation in Saccharomyces cerevisiae. Mol. Biol. Cell *18*, 557–568.

Von Hoff, D.D., Needham-VanDevanter, D.R., Yucel, J., Windle, B.E., and Wahl, G.M. (1988). Amplified human MYC oncogenes localized to replicating submicroscopic circular DNA molecules. Proc. Natl. Acad. Sci. USA *85*, 4804–4808.

Wang, E., Ballister, E.R., and Lampson, M.A. (2011). Aurora B dynamics at centromeres create a diffusion-based phosphorylation gradient. J. Cell Biol. *194*, 539–549.

Warsi, T.H., Navarro, M.S., and Bachant, J. (2008). DNA topoisomerase II is a determinant of the tensile properties of yeast centromeric chromatin and the tension checkpoint. Mol. Biol. Cell *19*, 4421–4433.

Wilkins, B.J., Rall, N.A., Ostwal, Y., Kruitwagen, T., Hiragami-Hamada, K., Winkler, M., Barral, Y., Fischle, W., and Neumann, H. (2014). A cascade of histone modifications induces chromatin condensation in mitosis. Science *343*, 77–80.

Xu, Z., Cetin, B., Anger, M., Cho, U.-S., Helmhart, W., Nasmyth, K., and Xu, W. (2009). Structure and function of the PP2A-shugoshin interaction. Mol. Cell *35*, 426–441.

Zhao, K., Chai, X., and Marmorstein, R. (2003). Structure of the yeast Hst2 protein deacetylase in ternary complex with 2′-O-acetyl ADP ribose and histone peptide. Structure *11*, 1403–1411.

Please cite this article in press as: Kruitwagen et al., Centromeres License the Mitotic Condensation of Yeast Chromosome Arms, Cell (2018), https://doi.org/10.1016/j.cell.2018.09.012

STAR★METHODS

KEY RESOURCES TABLE

REAGENT or RESOURCE	SOURCE	IDENTIFIER
Antibodies		
Rabbit polyclonal anti-Histone H3 (phospho S10)	Abcam	Cat#ab5176; RRID: AB_304763
Rabbit polyclonal anti-Histone H3	Abcam	Cat#ab46765; RRID: AB_880439
Chemicals, Peptides, and Recombinant Proteins		
Estradiol	Sigma-Aldrich	Cat#E8875
Alpha factor	GenScript	Cat#RP01002
Mouse IgG	Diagenode	Cat#C15400001-15
Zymolyase	AMS biotechnology	Cat#120491-1
Critical Commercial Assays		
QIAquick PCR purification kit	QIAGEN	Cat#28106
Power SYBR Green PCR Master Mix	Thermo Fisher Scientific	Cat#4368702
Dynabeads Protein A for Immunoprecipitation	Thermo Fisher Scientific	Cat#10001D
Dynabeads Protein G for Immunoprecipitation	Thermo Fisher Scientific	Cat#10003D
Deposited Data		
Raw and processed ChIP-seq data	This paper	GEO: GSE100643; https://www.ncbi.nlm.nih.gov/geo/query/acc.cgi?acc=GSE100643
*CEN4** Saccharomyces cerevisiae reference genome: Genome_before	This paper	GEO: GSE100643; https://www.ncbi.nlm.nih.gov/geo/query/acc.cgi?acc=GSE100643
cen4- Saccharomyces cerevisiae reference genome: Genome_after	This paper	GEO: GSE100643; https://www.ncbi.nlm.nih.gov/geo/query/acc.cgi?acc=GSE100643
Experimental Models: Organisms/Strains		
S. cerevisiae strain MATa trp1::TetO:TRP1 lys4::LacO:LEU2 his3::LacR-GFP:HIS3 TetR-mCherry	Neurohr et al., 2011	yYB3476
S. cerevisiae strain MATa Spc42-CFP:kanMX4 Gal4-EBD:TRP1 TetR:LEU2 pGAL-Rec:HIS3 ura3Δ0 met15 lys2 containing plasmid pPCM14 *(224 tetO-REC-URA3-CEN-REC-LEU2)*	Denoth-Lippuner et al., 2014b	yYB 6100
S. cerevisiae strain MATa Spc42-CFP:kanMX4 Gal4-EBD:TRP1 TetR:LEU2 pGAL-Rec:HIS3 ura met15 lys2 Ipl1-tetR-mCherry:hphNT1 containing plasmid pPCM14 *(224 tetO-REC-URA3-CEN-REC-LEU2)*	This paper	yYB 9203
S. cerevisiae strain MATa loxCEN4lox:KanMX GDP-creEDB78:LEU2 his3Δ1 leu2Δ0 ura3Δ0 met15Δ0	This paper	yYB 9867
S. cerevisiae strain MATa Spc42-CFP:kanMX4 Gal4-EBD:TRP1 TetR:LEU2 pGAL-Rec:HIS3 SHHF2-SHHT2S10D:hygNT1 ura met15 lys2 containing plasmid pPCM14 *(224 tetO-REC-URA3-CEN-REC-LEU2)*	This paper	yYB 10194
S. cerevisiae strain MATa Spc42-CFP:kanMX4 Gal4-EBD:TRP1 TetR:LEU2 pGAL-Rec:HIS3 SHHF2-SHHT2S10D:hygNT1 hst2::NatMX ura met15 lys2 containing plasmid pPCM14 *(224 tetO-REC-URA3-CEN-REC-LEU2)*	This paper	yYB 10257
S. cerevisiae strain MATa his3::HIS3 pGAL-Rec Nup82-3GFP:KAN TetR-mCherry:Kan Gal4-EBD:Trp Spc42-GFP:HIS ura3-52 ade2-101 containing plasmid pPCM14 *(224 tetO-REC-URA3-CEN-REC-LEU2)*	This paper	yYB 10761
S. cerevisiae strain MATa trp1::TetO:TRP1 lys4::LacO:hphNT1 his3::LacR-GFP:HIS3 TetR-mCherry loxCEN4lox:KanMX GDP-creEDB78:LEU2 ura3::CFP-TUB1:URA3 ade2 leu2	This paper	yYB 11181

(*Continued on next page*)

Continued

REAGENT or RESOURCE	SOURCE	IDENTIFIER
S. cerevisiae strain MATa trp1::TetO:TRP1 lys4::LacO:hphNT1 his3::LacR-GFP:HIS3 TetR-mCherry mad2::NatMX	This paper	yYB 11214
S. cerevisiae strain MATa trp1::TetO:TRP1 lys4::LacO:hphNT1 his3::LacR-GFP:HIS3 TetR-mCherry bub1::NatMX ura3 ade2 leu2	This paper	yYB 11224
S. cerevisiae strain MATa trp1::TetO:TRP1 lys4::LacO:hphNT1 his3::LacR-GFP:HIS3 TetR-mCherry sgo1::NatMX ura3 ade2 leu2	This paper	yYB 11324
S. cerevisiae strain MATα trp1::TetO:TRP1 lys4::LacO:hphNT1 his3::LacR-GFP:HIS3 TetR-mCherry mad2::NAT nnf1-17::LEU2 ura3::CFP-TUB1:URA3 ade2 leu2	This paper	yYB 11446
S. cerevisiae strain diploid trp1::TetO:TRP1 lys4::LacO:LEU2 his3::LacR-GFP:HIS3 TetR-mRFP / cen4lox:KanMX Rec:LEU2 ura3 ade2 leu2	This paper	yYB 11516
S. cerevisiae strain MATa trp1::TetO:TRP1 lys4::LacO:LEU2 his3::LacR-GFP:HIS3 TetR-mCherry ndc10-1 ura3::CFP-TUB1:URA3 ade2 leu2	This paper	yYB 11575
S. cerevisiae strain MATa trp1::TetO:TRP1 lys4::LacO:hphNT1 his3::LacR-GFP:HIS3 TetR-mCherry loxCEN4lox:KanMX GDP-creEDB78:LEU2 hht2-hhf2::[HHT-S10D-HHFS]-URA3 ura3 ade2 leu2	This paper	yYB 11743
S. cerevisiae strain diploid trp1::TetO:TRP1 lys4::LacO:hphNT1 his3::LacR-GFP:HIS3 TetR-mRFP loxCEN4lox:KanMX GDP-creEDB78:LEU2 ura3::CFP-TUB1:URA3 ade2 leu2 / his3Δ1 leu2Δ0 ura3Δ0 lys2Δ0	This paper	yYB 12158
S. cerevisiae strain MATa trp1::TetO:TRP1 lys4::LacO:LEU2 his3::LacR-GFP:HIS3 TetR-mCherry HHT2S10D:URA3 sgo1::NAT ura3 ade2 leu2	This paper	yYB 13300
S. cerevisiae strain MATa trp1::TetO:TRP1 lys4::LacO:LEU2 his3::LacR-GFP:HIS3 TetR-mCherry ura3 ade2 leu2 containing plasmid pMET25:IPL1-TetR-mCherry (ADE2)	This paper	yYB 13403
S. cerevisiae strain MATa trp1::TetO:TRP1 lys4::LacO:LEU2 his3::LacR-GFP:HIS3 TetR-mCherry ura3 ade2 leu2 containing plasmid pMET25:SGO1-TetR-mCherry (ADE2)	This paper	yYB 13405
S. cerevisiae strain MATa trp1::TetO:TRP1 lys4::LacO:hphNT1 his3::LacR-GFP:HIS3 TetR-mCherry sgo1::NatMX ura3 ade2 leu2 containing plasmid pMET25:SGO1-TetR-mCherry (ADE2)	This paper	yYB 13409
S. cerevisiae strain MATa trp1::TetO:TRP1 lys4::LacO:hphNT1 his3::LacR-GFP:HIS3 TetR-mCherry sgo1::NatMX ura3 ade2 leu2 containing plasmid pMET25:IPL1-TetR-mCherry (ADE2)	This paper	yYB 13417
S. cerevisiae strain MATa trp1::TetO:TRP1 lys4::LacO:hphNT1 his3::LacR-GFP:HIS3 TetR-mCherry loxCEN4lox:KanMX GDP-creEDB78:LEU2 ura3::CFP-TUB1:URA3 ade2 leu2 containing plasmid pMET25:IPL1-TetR-mCherry (ADE2)	This paper	yYB 13474
S. cerevisiae strain MATa trp1::TetO:TRP1 lys4::LacO:hphNT1 his3::LacR-GFP:HIS3 TetR-mCherry loxCEN4lox:KanMX GDP-creEDB78:LEU2 ura3::CFP-TUB1:URA3 ade2 leu2 containing plasmid pMET25:SGO1-TetR-mCherry (ADE2)	This paper	yYB 13476
S. cerevisiae strain MATa trp1::TetO:TRP1 lys4::LacO:LEU2 his3::LacR-GFP:HIS3 TetR-mRFP rts1::NatMX ura3 ade2 leu2 containing plasmid pMET25:IPL1-TetR-mCherry (ADE2)	This paper	yYB 13485
S. cerevisiae strain MATa ipl1-312 trp1::TetO:TRP1 lys4::LacO:LEU2 his3::LacR-GFP:HIS3 TetR-mCherry ura3 ade2 leu2 containing plasmid pMET25:SGO1-TetR-mCherry (ADE2)	This paper	yYB 13497
S. cerevisiae strain MATa ipl1-312 trp1::TetO:TRP1 lys4::LacO:LEU2 his3::LacR-GFP:HIS3 TetR-mCherry ura3 ade2 leu2 containing plasmid pMET25:IPL1-TetR-mCherry (ADE2)	This paper	yYB 13510
S. cerevisiae strain MATa trp1:TetO:TRP1 gpd-CreEBD78:LEU2 cen4::CEN1lox:KanMX ura3-52 his3Δ200 leu2 lys2-801 ade2-101 trp1Δ63	This paper	yYB 13587
S. cerevisiae strain MATa loxCEN4lox:KanMX GDP-creEDB78:LEU2 sgo1::NatMX his3 leu2 ura3 met15	This paper	yYB 13628

(*Continued on next page*)

Continued

REAGENT or RESOURCE	SOURCE	IDENTIFIER
S. cerevisiae strain MATa trp1::TetO:TRP1 lys4::LacO:hphNT1 his3::LacR-GFP:HIS3 TetR-mCherry loxCEN4lox:KanMX GDP-creEDB78:LEU2 hht2-hhf2::[HHT-S10D-HHFS]-URA3 hst2::NatMX ura3 ade2 leu2	This paper	yYB 13631
S. cerevisiae strain MATa trp1::LacO:TRP1 lys4::LacO:LEU2 his3::LacR-GFP:HIS3 ade2::NAT ura3 ade2 his3 leu2 trp1	This paper	yYB 13635
S. cerevisiae strain MATa trp1::LacO:TRP1 lys4::LacO:LEU2 his3::LacR-GFP:HIS3 ade2::NAT ura3 ade2 leu2 trp1 containing plasmid pMET25:SGO1-TetR-mCherry (ADE2)	This paper	yYB 13649
S. cerevisiae strain MATa trp1::LacO:TRP1 lys4::LacO:LEU2 his3::LacR-GFP:HIS3 ade2::NAT ura3 ade2 leu2 trp1 containing plasmid pMET25:IPL1-TetR-mCherry (ADE2)	This paper	yYB 13651
S. cerevisiae strain MATa trp1::TetO:TRP1 lys4::LacO:LEU2 his3::LacR-GFP:HIS3 TetR-mCherry dam1-1 mad2::NAT ura3 ade2 leu2	This paper	yYB 13732
S. cerevisiae strain MATa Spc42-CFP:kanMX4 Gal4-EBD:TRP1 TetR:LEU2 pGAL-Rec:HIS3 rts1::HYG ura3 met15 lys2 containing plasmid pPCM14 *(224 tetO-REC-URA3-CEN-REC-LEU2)*	This paper	yYB 13764
S. cerevisiae strain MATa trp1::TetO:TRP1 lys4::LacO:LEU2 his3::LacR-GFP:HIS3 TetR-mRFP rts1::NatMX sgo1::KanMX ura3 leu2	This paper	yYB 13847
S. cerevisiae strain MATa trp1::TetO:TRP1 lys4::LacO:LEU2 his3::LacR-GFP:HIS3 TetR-mCherry hst2::KanMX ade2::NatMX ura3 ade2 leu2 containing plasmid pMET25:SGO1-TetR-mCherry (ADE2)	This paper	yYB 13942
S. cerevisiae strain MATa trp1::TetO:TRP1 lys4::LacO:LEU2 his3::LacR-GFP:HIS3 TetR-mCherry hst2::KanMX ade2::NatMX ura3 ade2 leu2 containing plasmid pMET25:IPL1-TetR-mCherry (ADE2)	This paper	yYB 13943
S. cerevisiae strain MATa trp1::TetO:TRP1 lys4::LacO:LEU2 his3::LacR-GFP:HIS3 TetR-mCherry hht1::hht1-S10A:KanMXloxP hht2::hht2-S10A:bleloxP ura3 ade2 leu2 containing plasmid pMET25:SGO1-TetR-mCherry (ADE2)	This paper	yYB 13955
S. cerevisiae strain MATa trp1::TetO:TRP1 lys4::LacO:LEU2 his3::LacR-GFP:HIS3 TetR-mRFP SGO1-Y47A/Q50A/S52A ura3 ade2 leu2	This paper	yYB 14102
S. cerevisiae strain MATa his3::HIS3 pGAL-Rec TetR-mCherry:Kan Gal4-EBD:Trp ura3-52 ade2-101 Spc42-GFP:HygR pPCM14 *(224 tetO-REC-URA3-CEN-REC-LEU2)*	This paper	yYB 14157
S. cerevisiae strain MATa trp1::TetO:TRP1 lys4::LacO:LEU2 his3::LacR-GFP:HIS3 TetR-mRFP ctf19::NatMX ura3 ade2 leu2	This paper	yYB 14237
S. cerevisiae strain MATa trp1::TetO:TRP1 lys4::LacO:LEU2 his3::LacR-GFP:HIS3 TetR-mRFP chl4::NAT ura3 ade2 leu2	This paper	yYB 14310
S. cerevisiae strain MATa trp1::TetO:TRP1 lys4::LacO:hphNT1 his3::LacR-GFP:HIS3 TetR-mCherry loxCEN4lox:KanMX GDP-creEDB78:LEU2 ura3::CFP-TUB1:URA3 ade2 leu2 containing plasmid pMET25:IPL1-LacI-GFP (ADE2)	This paper	yYB 14413
S. cerevisiae strain MATa trp1::TetO:TRP1 lys4::LacO:hphNT1 his3::LacR-GFP:HIS3 TetR-mCherry leu2::Cre-EBD:LEU2 Shs1-loxPmCherry:Cln2 (3′UTR)-NatNT2-loxP-GFP ade2 leu2	This paper	yYB 14417
S. cerevisiae strain MATa trp1::TetO:TRP1 lys4::LacO:hphNT1 his3::LacR-GFP:HIS3 TetR-mRFP loxCEN4lox:KanMX GDP-creEDB78:LEU2 ura3::CFP-TUB1:URA3 ade2 leu2 containing plasmid pMET25:SGO1-LacI-GFP (ADE2)	This paper	yYB 14586
S. cerevisiae strain MATa trp1::TetO:TRP1 lys4::LacO:hphNT1 his3::LacR-GFP:HIS3 TetR-mRFP loxCEN4lox:KanMX GDP-creEDB78:LEU2 ura3::CFP-TUB1:URA3 ade2 leu2 containing plasmid pMET25:IPL1-D227A-TetR-mCherry (ADE2)	This paper	yYB 14594
S. cerevisiae strain MATa trp1::TetO:TRP1 lys4::LacO:hphNT1 his3::LacR-GFP:HIS3 TetR-mRFP loxCEN4lox:KanMX cdc15-1 ura3::Cre-EBD:LEU2 ura3 ade2 leu2	This paper	yYB 14639

(*Continued on next page*)

Continued

REAGENT or RESOURCE	SOURCE	IDENTIFIER
S. cerevisiae strain MATa trp1::TetO:TRP1 lys4::LacO:hphNT1 his3::LacR-GFP:HIS3 TetR-mRFP loxCEN4lox:KanMX dam1-1 mad2::NAT ura3::Cre-EBD:LEU2 ura3 ade2 leu2	This paper	yYB 14640
S. cerevisiae strain MATa trp1::TetO:TRP1 lys4::LacO:LEU2 his3::LacR-GFP:HIS3 TetR-mRFP ura3::CFP-TUB1:URA3 scc1-73:NAT mad2::HYG ade2 leu2	This paper	yYB 14641
S. cerevisiae strain MATa Spc42-CFP:kanMX4 Gal4-EBD:TRP1 TetR:LEU2 pGAL-Rec:HIS3 SHHF2-SHHT2S10D:hygNT1 sgo1::NatMX ura met15 lys2 containing plasmid pPCM14 *(224 tetO-REC-URA3-CEN-REC-LEU2)*	This paper	yYB 14836
S. cerevisiae strain MATa Spc42-CFP:kanMX4 Gal4-EBD:TRP1 TetR:LEU2 pGAL-Rec:HIS3 rts1::HYG sgo1::NAT ura3 met15 lys2 containing plasmid pPCM14 *(224 tetO-REC-URA3-CEN-REC-LEU2)*	This paper	yYB 14886
S. cerevisiae strain MATa Spc42-CFP:kanMX4 Gal4-EBD:TRP1 TetR:LEU2 pGAL-Rec:HIS3 SGO1-Y47A/Q50A/S52A ura3 met15 lys2 containing plasmid pPCM14 *(224 tetO-REC-URA3-CEN-REC-LEU2)*	This paper	yYB 14889
S. cerevisiae strain diploid trp1:TetO:TRP1 gpd-CreEBD78:LEU2 cen4::CENlox:KanMX / TetR-mRFP TetR-GFP:LEU2 ura3-52 his3Δ200 leu2 lys2-801 ade2-101 trp1Δ63	This paper	yYB 14890
S. cerevisiae strain diploid Spc42-CFP:kanMX4 Gal4-EBD:TRP1 TetR-GFP:LEU2 pGAL-Rec:HIS3 ura3 met15 lys2 / his3::HIS3 pGAL-Rec TetR-mCherry:Kan Gal4-EBD:Trp ura3-52 ade2-101 containing plasmid pPCM14 *(224 tetO-REC-URA3-CEN-REC-LEU2)*	This paper	yYB 14891
S. cerevisiae strain MATa Spc42-CFP:kanMX4 Gal4-EBD:TRP1 TetR:LEU2 pGAL-Rec:HIS3 SGO1-Y47A/Q50A/S52A hst2::hphNT1 ura3 met15 lys2 containing plasmid pPCM14 *(224 tetO-REC-URA3-CEN-REC-LEU2)*	This paper	yYB 14892
S. cerevisiae strain MATα trp1::TetO:TRP1 lys4::LacO:LEU2 his3::LacR-GFP:HIS3 TetR-mRFP HST2-I117A ura3 ade2 leu2	This paper	yYB 14894
S. cerevisiae strain trp1::TetO:TRP1 lys4::LacO:LEU2 his3::LacR-GFP:HIS3 TetR-mRFP HTA1-S121A HTA2-S121A ura3 ade2 leu2	This paper	yYB 14903
S. cerevisiae strain MATa trp1::TetO:TRP1 lys4::LacO:hphNT1 his3::LacR-GFP:HIS3 TetR-mRFP bub1::NatMX ura3 ade2 leu2 containing plasmid pMET25:SGO1-TetR-mCherry (ADE2)	This paper	yYB 14904
S. cerevisiae strain MATα Spc42-CFP:kanMX4 Gal4-EBD:TRP1 TetR:LEU2 pGAL-Rec:HIS3 bub1::hphNT1 SGO1-Y47A/Q50A/S52A ura3 met15 lys2 containing plasmid pPCM14 *(224 tetO-REC-URA3-CEN-REC-LEU2)*	This paper	yYB 14914
S. cerevisiae strain MATa trp1::TetO:TRP1 lys4::LacO:LEU2 his3::LacR-GFP:HIS3 TetR-mRFP SGO1-Y47A/Q50A/S52A bub1::hphNT1 ura3 ade2 leu2	This paper	yYB 14917
S. cerevisiae strain MATa trp1::TetO:TRP1 lys4::LacO:LEU2 his3::LacR-GFP:HIS3 TetR-mRFP rts1::NatMX bub1::hphNT1 ura3 ade2 leu2	This paper	yYB 14918
S. cerevisiae strain MATa Spc42-CFP:kanMX4 Gal4-EBD:TRP1 TetR:LEU2 pGAL-Rec:HIS3 rts1::HYG bub1::NAT ura3 met15 lys2 containing plasmid pPCM14 *(224 tetO-REC-URA3-CEN-REC-LEU2)*	This paper	yYB 14932
S. cerevisiae strain MATa his3Δ200 leu2Δ0 lys2Δ0 trp1Δ63 ura3Δ0 met15Δ0 can1::MFA1pr-HIS3 hht1-hhf1::NatMX4 hht2-hhf2::[HHTS-S10D-HHFS]*-URA3	Dharmacon	https://dharmacon.horizondiscovery.com/cdnas-and-orfs/non-mammalian-cdnas-and-orfs/yeast/yeast-synthetic-histone-and-h4-mutant-collection/
Oligonucleotides		
Sequences are provided in Table S3	N/A	N/A
Recombinant DNA		
Plasmid pPCM14 *(224 tetO-REC-URA3-CEN-REC-LEU2)*	Megee and Koshland, 1999	N/A
Plasmid pMET25:IPL1-TetR-mCherry ADE2	This paper	N/A
Plasmid pMET25:SGO1-TetR-mCherry ADE2	This paper	N/A

(*Continued on next page*)

Continued

REAGENT or RESOURCE	SOURCE	IDENTIFIER
Plasmid pMET25:IPL1-LacI-GFP ADE2	This paper	N/A
Plasmid pMET25:SGO1-LacI-GFP ADE2	This paper	N/A
Plasmid pMET25:IPL1-D227A-TetR-mCherry ADE2	This paper	N/A
Plasmid pML104	Laughery et al., 2015	N/A
Software and Algorithms		
ImageJ (Fiji)	NIH	https://imagej.nih.gov/ij/
softWoRX	GE Healthcare	N/A
GraphPad Prism	GraphPad	https://www.graphpad.com/
TillVision	Thermo Fisher Scientific	https://www.fei.com/home/
bowtie version 2.2.9	Langmead and Salzberg, 2012	http://bowtie-bio.sourceforge.net/bowtie2/index.shtml
bedtools multicov	Quinlan and Hall, 2010	http://bedtools.readthedocs.io/en/latest/content/tools/multicov.html
Other		
ChIP-seq raw reads processing and alignment to genome_before or genome_after	Hemispherian AS	https://www.genomestream.com/home/

CONTACT FOR REAGENT AND RESOURCE SHARING

Comments and/or requests for resources and/or reagents should be directed to and will be fulfilled by the Lead Contact, Yves Barral (yves.barral@bc.biol.ethz.ch).

EXPERIMENTAL MODEL AND SUBJECT DETAILS

Strains and media

All yeast strains used in this study are isogenic to the S288c genetic background, unless otherwise mentioned. One representative clone of each mutant is listed in the Key Resources Table. Microbiological methods were performed according to standard procedures. The H3S10D mutant cassette was obtained from the synthetic non-essential histone collection from Dharmacon (Dai et al., 2008). Strains were obtained by tetrad dissections (2:2 segregation of all markers, temperature sensitivity and mating types was always verified) and/or transformation of PCR-derived chromosomal integration cassettes (Longtine et al., 1998; Janke et al., 2004). For the latter, a DNA fragment containing 50 base pairs homology in front of the start codon of the gene of interest and 50 base pairs homology after the stop codon of said gene with an auxotrophic or resistance cassette in between was generated by PCR and transformed in budding yeast. Cells were plated on selective medium and up to eight clones were streaked for single colonies. Genomic DNA was extracted and deletions were confirmed by PCRs: one reaction to test for absence of the gene of interest and another for presence of the deletion cassette. To ensure the absence of suppressor mutations, single deletion strains were backcrossed once to WT S288c. Temperature sensitive mutations were introduced by crossing and tetrad dissection. HST2-I117A, H2A-S121A and Sgo1-3A alleles were introduced by CRISPR/Cas9 genome editing (see below) (Laughery et al., 2015). The excisable centromere on chromosome IV was obtained from Warsi et al. (2008). In short, the native *CEN4* was replaced by *CEN1,* followed by a kanamycin resistance cassette, flanked by lox recombination sites. This is referred to as *CEN4**.

All WT and mutant strains were grown at 30°C in YPD, with the exception of temperature sensitive mutant strains, which were grown at 25°C for daily culturing. Temperature sensitive strains were shifted to their restrictive temperatures directly (i.e., without synchronization in G1) and allowed to pass one cell cycle (90-100 minutes) prior to imaging (see below); *dam1-1* (35°C), *nnf1-17* (33°C), *cdc15-1* (37°C), with the exception of *ipl1-321, ndc10-1* and *scc1-73* containing strains, which were released at their restrictive temperatures after alpha-factor mediated G1 arrest (see below).

Expression of TetR-mCherry or LacI-GFP fusion proteins from the repressible MET25 promoter was achieved by initially growing cells overnight in SD –ADE medium to OD600 = 0.8. Next, cells were spun down, washed in 5x volume SD –ADE –MET and finally released in a volume equal to the starting volume of SD –ADE –MET. Cells were imaged after 3 hours (see below).

Cells containing the model DNA circle pPCM14 were grown in SD –URA overnight to OD600 > 1.0, to select for maintenance of the (CEN+) circle. In the morning, cells were diluted in YPD to OD600 = 0.15 and imaged after 3-4 hours. To induce excision of the centromere, estradiol was added after 1 hour (*cen-* circle data) or the culture was left unperturbed for the same time (*CEN+* circle data).

For ChIP assays, log phase cultures at 30°C were used, with the exception of *cdc15-1* and *ipl1-321* strains (Figure S6), for which cells were shifted to 37°C for 2 and 3 hours, respectively.

METHOD DETAILS

CRISPR/Cas9 mediated introduction of point mutations

gRNAs were designed using the online tool at http://wyrickbioinfo2.smb.wsu.edu/crispr.html, cloned into the pML104 vector and transformed in yeast together with a PCR-derived repair template containing the mutation(s) of interest (Laughery et al., 2015). Clones were picked and verified by PCR and sequencing.

Alpha-factor-mediated G1 arrest

To ensure proper cell cycle staging and/or proper inactivation of certain temperature-sensitive alleles (see below), data from *WT CEN4** and *cen4-* cells in Figures 1D and 1E (all 8 and six columns, respectively) and Figures S3A and S3B, *ipl1-321* (Figure 1E), *ndc10-1* and *scc1-73* mutant strains (both Figures 3E and 3F), stems from cells initially synchronized in G1 with alpha-factor.

For this, WT exponentially growing cells in liquid YPD medium at OD600 = 0.3 were obtained and 2 μg/ml alpha-factor (Genscript) was added. After 45 minutes, an identical amount was re-added. After another 45 minutes, we added 1 μg/ml alpha-factor. After a total of 150 minutes, G1-arrest was confirmed by visual inspection (i.e., cells were small and unbudded, indicating they are in G1 phase) using a bright field microscope. Cells were spun down (650 RCF, 3 minutes, room temperature), washed in 5x volume YPD medium without alpha-factor and released at the desired temperature until anaphase was reached (as judged by visual inspection using a bright field microscope: the majority of cells had buds and unbudded or small-budded cells were largely absent; generally, after 90-120 minutes). For strains carrying the *ipl1-321* (Figure 1E) or *ndc10-1* (Figure 3E) alleles, the exact same procedure was performed, except that these were grown and arrested at 25° (permissive temperature), but released at 35°C (restrictive temperature). *scc1-73* cells (Figure 3E) were released at 25°C, but switched to 35°C in metaphase (as judged by visual inspection at a bright field microscope; generally, 45 minutes after release from alpha-factor arrest).

CEN4* excision

Unless otherwise indicated, in strains expressing the Cre recombinase fused to the estradiol-binding domain, *CEN4** excision was performed by adding 1 μM of estradiol (Sigma-Aldrich) from a 1000x concentrated stock dissolved in ethanol to exponentially growing cells in liquid YPD medium.

For alpha-factor synchronized *CEN4** strains, which were used to obtain data in Figures 1D, 1E, S3, and S4, estradiol was added together with the third round of alpha-factor addition (see above), to obtain *cen4-* G1-synchronized cells. Subsequently, these cells were released in YPD medium containing estradiol and imaged at different times to obtain cells of the desired cell cycle stage.

CEN4* excision efficiency assay

Strains expressing the Cre recombinase fused to the estradiol-binding domain were treated with estradiol (Sigma-Aldrich) for 3 hours before isolation of genomic DNA (gDNA) as following. Cell walls were degraded using Zymolyase (10 mg/ml, AMS biotechnology) in a cell ressuspension buffer [50 mM KH_2PO_4 (pH 7.5), 1.2 M sorbitol] for 30 min at 30°C, before addition of lysis buffer [100 mM Tris (pH 8.0), 50 mM EDTA, 1% SDS v/v]. Proteins were then precipitated using sodium acetate (final concentration 1.1 M). After centrifugation at 14000 rpm, the supernatent was transferred to a new tube and the gDNA was precipitated using isopropanol. After centrifugation at 14000 rpm, pelleted gDNA was washed using 70% ethanol. After centrifugation at 14000 rpm, the pelleted gDNA was dried and ressuspended in TE buffer [10 mM Tris (pH 8.0), 1 mM EDTA] containing RNase DNase free (Merck, 04716728001), and incubated overnight at room temperature.

To address *CEN4**-excision efficiency, gDNA samples were analyzed by qPCR using the Power SYBR Green PCR Master Mix (Thermo Fisher Scientific) and the StepOnePlus real-time PCR system (Thermo Fisher Scientific) using specific oligonucleotides (see Figure S1; Table S3).

Construction and excision of lox:mCherry:NatMX:lox:GFP

Introduction of the lox:mCherry:NatMX:lox:GFP cassette at the *SHS1* locus was performed by PCR-based chromosomal integration (Lengefeld et al., 2017). A PCR product containing homology with 50 basepairs in front of the SHS1 stop codon and 50 basepairs homology after the stop codon with the lox:mCherry:NatMX:lox:GFP cassette in between was generated and transformed in budding yeast. Clones were verified by PCR and fluorescence. Excision of mCherry:NatMX from the *SHS1*:lox:mCherry:NatMX:lox:GFP locus was performed by adding the appropriate amount of estradiol from a 1000x stock dissolved in ethanol on exponentially growing cells and confirmed after 100 minutes by fluorescence microscopy, when cells displayed green as well as red fluorescence (see Figure S5).

Microscopy

To obtain chromosome contraction and compaction data, cells were imaged exactly as described before (Kruitwagen et al., 2015): Cells were resuspended in non-fluorescent SD-TRP medium and put on a SD -TRP 2% agar pad containing non-fluorescent medium. All microscopy was done with a Deltavision microscope (Applied Precision) equipped with a CCD HQ2 camera (Roper), 250W Xenon lamps, Softworx software and a temperature chamber. A stack containing 10 0.5 μm Z-slices was recorded in the transmission, FITC, TRITC and/or CFP channels. Images were deconvolved using Softworx software and processed using Fiji software. For FRET experiments, fluorophores were excited with FITC and emission in the TRITC channel was recorded. Subsequently, standard FITC-FITC

and TRITC-TRITC excitation and emission was performed. Using Fiji software, ROIs were drawn around foci of sum intensity projections and FRET emission intensity over total TRITC intensity was calculated.

For circle propagation assays, an Olympus BX50 microscope with a Piezo motor, Monochromator light source, Andor CCD camera and TillVision software was used. Images were acquired using a 100x, 1.4 NA objective, 2x2 binning with 10 Z slices of 0.5 μm in CFP and GFP or RFP and GFP channels. Maximum intensity projections were made using Fiji software.

For all example microscopy images shown in this manuscript (circle propagation, chromosome contraction and compaction), maximum Z projections from deconvolved images were used. For visibility, contrast and brightness were adjusted for each individual cell. Thus, example images do not reflect absolute fluorescence intensities as measured for chromatin compaction, but rather serve to display cell morphology and chromosomal localization. Individual example cell images were spliced together.

DNA circle propagation assay

For imaging, 1-1.5 mL of culture was spun down (1.5min 650RCF at room temperature) in an Eppendorf tube and the pellet was washed in 1x PBS before being resuspended in non-fluorescent medium (SD –TRP) and put on a glass slide and coverslip. Cells treated with estradiol contained 1-4 foci of DNA circles, confirming they underwent approximately 1-2 cell cycles after *CEN* excision (Denoth-Lippuner et al., 2014a).

ChIP-seq and ChIP-qPCR experiments

Prior to ChIP-seq experiments, we compared two antibodies specific for H3-pS10 (ab5176, Abcam and Millipore-04-817) in ChIP-qPCR experiments. Although very similar results were obtained for both antibodies (namely, much less signal on chromosome arm loci as compared to centromere-proximal loci), we decided to use ab5176, as it gave a much better signal to noise ratio (data not shown). The fact that both these antibodies showed similar depletion of S10 phosphorylation on chromosome arms indicated that the lack of the S10 signal on the arms was not due to additional, masking modifications on K9. Indeed, unlike ab5176 the antibody Millipore-04-817 is poorly sensitive to K9 modification (Rothbart et al., 2015).

For ChIP assays, log phase cultures at 30°C were used, with the exception of *cdc15-1* and *ipl1-321* strains (Figure S6), for which cells were shifted to 37°C for 2 and 3 hours, respectively (Chymkowitch et al., 2017, 2015). Cells were fixed with 1% (vol/vol) formaldehyde for 30 min. Formaldehyde was quenched for 5 min by adding glycine to a final concentration of 125 mM. Cells were washed with cold Tris-buffered saline, resuspended in lysis buffer [50 mM HEPES-KOH (pH 7.5), 140 mM NaCl, 1 mM EDTA, 1% (vol/vol) Triton X-100, 0.1% (vol/vol) Na-deoxycholate, and protease inhibitor cocktail] and were sonicated twice for 15 min by performing alternating cycles of 30 s pulses followed by a 30 s cool-down period using a Diagenode Bioruptor Twin. After centrifugation, supernatants were immunoprecipitated at 4°C using anti-H3-pS10 (ab5176) and pan-H3 (ab46765) antibodies and protein A and G Dynabeads (Thermo Fisher Scientific, 10001D and 10003D). Control ChIPs were performed using mouse IgG from Diagenode (C15400001-15) and Dynabeads (Thermo Fisher Scientific, 10001D and 10003D). Beads were first washed with lysis buffer, followed by washing with lysis buffer containing 500 mM NaCl, then with wash buffer [10 mM Tris (pH 8.0), 250 mM LiCl, 0.5% (vol/vol) Nonidet P-40, 0.5% (wt/vol) Na-deoxycholate and 1 mM EDTA], and finally with a buffer (pH 8.0) containing 10 mM Tris and 1 mM EDTA. Elution was performed in 50 mM Tris (pH 8.0), 10 mM EDTA, 1% (wt/vol) SDS at 65°C, and the cross-link was reversed 5 hours at 65°C. After RNase DNase free (Merck, 04716728001) and proteinase K treatment (Merk, 03115828001), DNA fragments were purified using QIAquick PCR purification kit (QIAGEN). Novogene performed high-throughput sequencing of purified DNA fragments. For ChIP-qPCR, DNA fragments were amplified by qPCR using the Power SYBR Green PCR Master Mix (Thermo Fisher Scientific) and the StepOnePlus real-time PCR system (Thermo Fisher Scientific). Oligonucleotides used for qPCR experiments are described in Table S3 and Chymkowitch et al. (2012).

QUANTIFICATION AND STATISTICAL ANALYSIS

DNA compaction and contraction analysis

Analyses were performed as in Kruitwagen et al. (2015): For long-range contraction, maximum projections were made and measurements were done in 2D. The rationale for this being that the anaphase nucleus is rotationally symmetric and elongates in the X-Y plane of imaging, or close to it, aligning the chromosomes on that plane. Thus, measurements made on the projection plane only slightly underestimate the length of these chromosomes. Only distances measured on unattached chromosomes, which do not necessarily lay on the X-Y plane, may be more significantly underestimated. The fact that *cen-* chromosomes showed a longer *TRP1-LYS4* distance than *WT* ones, and not the opposite, strengthens the conclusion that these chromosomes fail to condense. Therefore, in this microscopy setup, 2D measurements were sufficient for drawing conclusions. Contraction was then determined by drawing a straight line from the center of the TetR-mCherry (red) focus to that of the LacI-GFP (green) focus in the mother cell. *cen4-* anaphase cells were identified by the presence of a mitotic (anaphase) spindle and only one focus in at least one channel (TRITC or FITC). When needed, nuclear outline was determined by increasing the contrast of the mCherry channel. For short-range compaction, the same microscopy images were used to make sum intensity projections. G1-phase cells were identified by small, round, unbudded morphology of the cells. Late anaphase cells were identified by the presence of a 4-9 μm long mitotic spindle, labeled by CFP-Tub1, and/or by the presence of a fluorescently tagged sister chromatid oriented along the mother-bud axis of the cell. A circular region of interest (ROI) was drawn around a green or red (mother cell) focus in Fiji Software and an identically sized ROI was placed next

to it to measure background fluorescence. Focus and background intensities were measured, after subtraction of the latter from the first, leading to the background corrected fluorescence intensity. Compaction data was normalized to WT G1 values (i.e., the average fluorescence intensity of TetR-mCherry and LacI-GFP foci in WT G1 cells was set to 100 arbitrary units).

Statistics for microscopy experiments

Microscopy data graphs from each mutant strain represent pooled data points of three independent clones of identical genotype (''biological replicates''; indicated by white circles for contraction and black dots for compaction), unless otherwise indicated. Exceptionally, for WT strains, or strains published before, we show technical replicates (indicated by gray dots for contraction and compaction). For the commonly used *ipl1-321* strain, we show no technical replicates in G1 and only 2 for anaphase. Data of biological or technical replicates was pooled prior to significance testing. For datasets containing < 3 mutants, Student's t tests were performed to test for significance. For datasets of 3 or more strains, Shapiro-Wilk tests were performed to test datasets for normality. Subsequently, Kruskal-Wallis tests were performed to test for statistical significance of data.

DNA circle propagation frequency calculations

Circle propagation frequencies were calculated by first determining the frequency of cells that retain all circle foci in the mother compartment during mitosis (with ''a'' for all the ''x'' cells containing one circle focus, ''b'' for all the ''y'' cells containing 2 circle foci and ''c'' for all ''z'' cells containing 4 circle foci; x, y and z being the total number of cells with one, two or four circles, respectively. The total number of cells for each clone per mutant is well above 100). Next, we used these numbers to calculate the circle propagation frequency. For example, retaining 2 circles in the mother cell is not a single event, but requires the retention of two individual circles. Therefore, the distribution is binomial. For the cells with two circles, the frequency of cells with two circles in the mother cell is then f^2, the frequency of cells with 1 circle in the mother cell is 2f(1-f) and the frequency of cells with no circles in the mother cell is $(1-f)^2$, where f is the retention frequency in the mother cell per circle and $f^2 + 2f(1-f) + (1-f)^2 = 1$. Thus, for cells with 2 circles (2 dots), the frequency of circle retention in the mother cell (per circle) f is the square root of the frequency b at which we observe cells with both circles in the mother cell among all the y cells with two circles: $f = \sqrt{b}$. For cells with four circles (four dots) the equation reads now $f^4 + 4f^3(1-f) + 6f^2(1-f)^2 + 4f(1-f)^3 + (1-f)^4 = 1$, where $f^4 = c$, the frequency of the cells with all four circles in the mother cell among all cells with four circles, etc… Thus, in this case, $f = \sqrt[4]{c}$. To evaluate f most accurately, we make the average of the values that we obtain from the data gained from all x cells with one dot, all y cells with two dots and all z cells with four dots, weighted by the total number of circle counted in each category. For example, there are 1x circles in all the cells with one circle, 2y circles in the cells with two circles and 4z cells all cells with four circles. This gives us the equation: $< f > = (xa+2y\sqrt{b}+4z\sqrt[4]{c})/(x+2y+4z)$. Accordingly, the frequency of passage into the daughter cell is $1- < f >$, and expressed as a percentage it is $100(1- < f >)$.

Analysis of ChIP sequencing data

Processing of raw reads was performed by Hemispherian AS (https://www.genomestream.com/home/) (Chymkowitch et al., 2017). Two recombinant genomes including chromosome IV-specific sequences of *CEN4** (genome_before) and *cen4-* (genome_after) cells were generated (GEO: GSE100643). The sequence present in *CEN4** cells removed after estradiol treatment was cut out and replaced by the remaining sequence found in *cen4-* cells. A new reference genome annotation adjusted for changes in chromosome name and position was also generated. Chromosome IV *CEN+* coordinates were added 3207bp if they were located downstream of the first cut site (449257), because the insert is 4164bp minus 975bp longer than the sequence of a *WT* chromosome IV. Similarly, coordinates of *cen4-* chromosome IV were subtracted 310 bp (647-957). Raw read generated from *CEN4** and *cen4-* cells were then aligned to the corresponding genome using bowtie version 2.2.9 using parameters-best. We also generated chromosome size files and genome files for IGV visualization.

Quantification of ChIP-seq reads on whole chromosomes was performed by Hemispherian AS. Each yeast chromosome was divided in 500 equally sized bins. The number of reads in each bin for IP and input samples was quantified using bedtools multicov, and normalized the values for sequencing depth before subtracting the input values.

Reads were counted separately for samples not treated and treated with estradiol (because they have different headers) by dividing each chromosome in 500 equally sized bins. Samples were then merged, column headers added and normalized to sequencing depth (Table S1). A 40Kb-long region containing *CEN4* and the TetO array was divided in 300 equally sized bins and ChIP-seq reads were quantified as described above (Table S2).

For H3-pS10 ChIPs specific controls and normalization measures have been applied. We aligned the reads coming from inputs and IPs for H3, H3-pS10 and IgG IPs in *WT* and *H3-S10A* (a mutant strain expressing non-phosphorylatable H3-S10A). Next, we subtracted the background noise signal of the IgG ChIPs from the H3-pS10 and H3 ChIPs for both *WT* and *H3-S10A* cells. We then normalized the signal coming from H3-pS10 ChIPs to total H3. Finally, since the signal observed in the *H3-S10A* cells can be considered as background noise for H3-pS10 ChIPs, we removed this noise from the signal coming from H3-pS10 ChIPs in *WT* cells. These experiments were performed in triplicates.

DATA AND SOFTWARE AVAILABILITY

The accession number for ChIP-sequencing data reported in this paper is GEO: GSE100643.

Cell

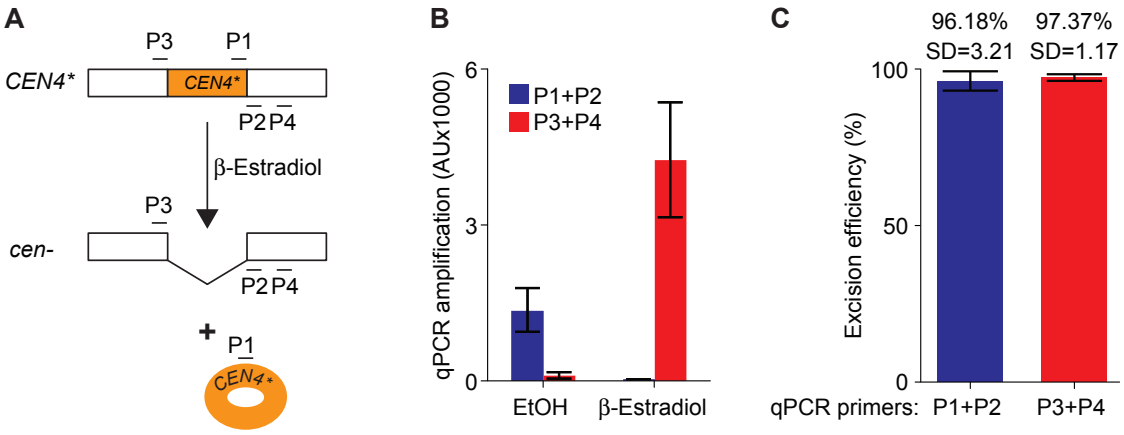

Figure S1. *CEN4 Excision Frequency as Determined by qPCR, Related to Figure 1**

(A) Diagram depicting the strategy for addressing *CEN4** excision upon β-estradiol treatment. qPCR primer 1 (P1) combined with primer 2 (P2) only give an amplification product in *CEN4** cells, while primer 3 (P3) and primer 4 (P4) allow amplification only in *cen4-* cells.

(B) Result of the qPCR-based excision efficiency assay described in (A).

(C) Calculation of *CEN4** excision efficiency. For P1+P2, the qPCR product was obtained in 96.18% of *CEN4** cells, while after 3 hours in β-estradiol this product was only detected in 3.82% of cells. For P3+P4, the qPCR product was obtained in 97.37% of *cen4-* cells, while before treatment with β-estradiol this product was only detected in 2.63% of *CEN4** cells.

In (B) and (C) error bars represent the SEM of four independent experiments.

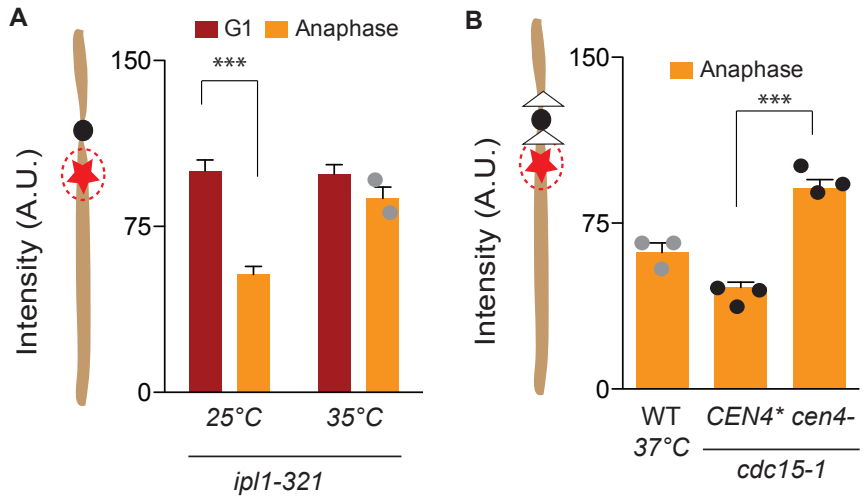

Figure S2. Chromatin Compaction in *ipl1-321* and *cdc15-1* Mutant Cells, Related to Figure 1

(A) Fluorescence intensity of the TetO-TetR-mCherry locus in *ipl1-321* cells at the indicated temperature in G1 or anaphase. Student t tests were performed to test significance. *$p < 0.05$, **$p < 0.01$, ***$p < 0.001$, non-significance not shown.

(B) Fluorescence intensity of the TetO-TetR-mCherry locus in *cdc15-1* and *WT* cells grown at the indicated temperature. *WT* at the restrictive temperature from Figure 3F for reference. Circles, statistics and graph layout as in Figure 1.

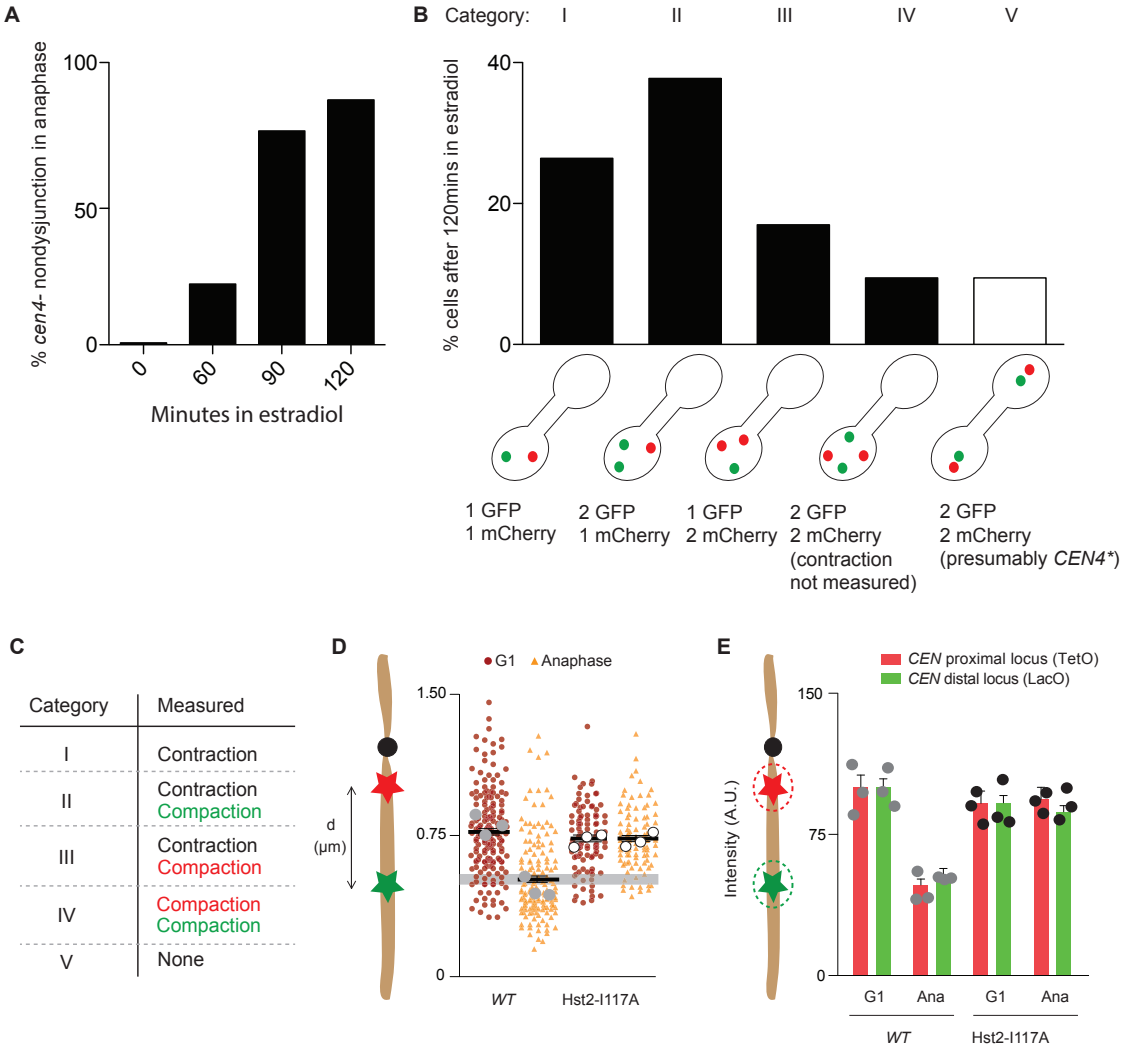

Figure S3. Categorization of Phenotypes of *cen4*–Containing Cells, Related to Figure 1

(A) *LoxCEN4** excision frequencies after induction of recombination. Anaphase cells (as judged by Tub1-CFP) containing the *cen4-* chromosome (as determined by the presence of mCherry and GFP foci in the mother cell).

(B) Fraction of anaphase cells with an indicated distribution of green and red foci 120 minutes after induction of *LoxCEN4** excision.

(C) Condensation measurements that were performed in cells of the indicated category shown in B. The color of the word "compaction" indicates the color of the focus/foci that was measured.

(D and E) Contraction (D) and compaction (E) data in the indicated cell cycle stages in *WT* and cells containing the Hst2-I117A mutation. *WT* repeated from Figures 5D and 5E for reference. Circles, statistics and graph layout as in Figure 1.

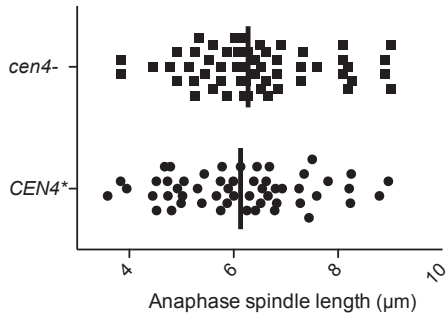

Figure S4. Anaphase Spindle Length Is Indistinguishable between *CEN4 and *cen4-* cells, Related to Figure 1**

Anaphase spindle length (μm) in cells containing a *CEN4** or *cen4-* chromosome. Shown is the median spindle length.

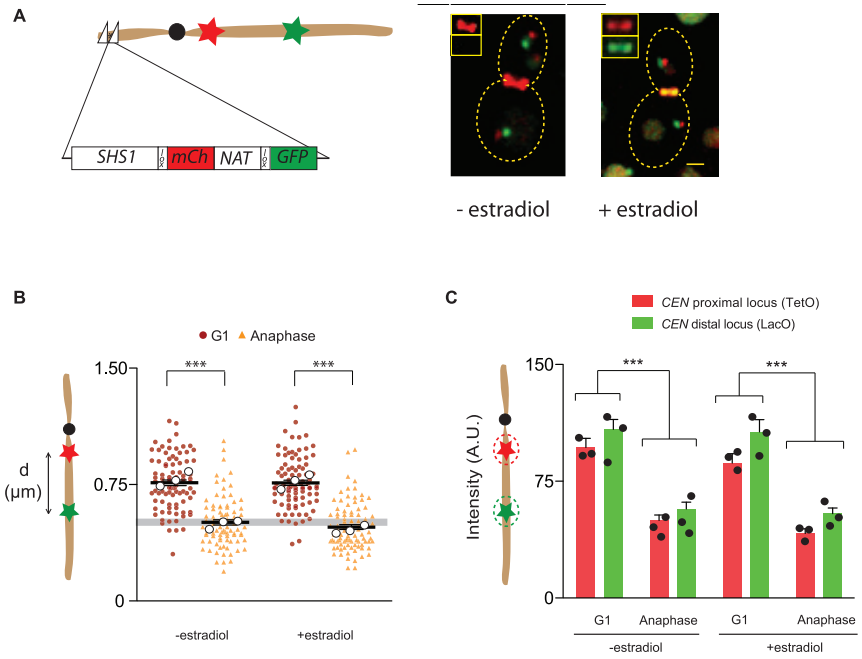

Figure S5. Excision of a Non-*CEN4 Piece from Chromosome IV Does Not Impact Its Condensation, Related to Figure 1**

(A) Strategy to lox out mCherry:NAT from the left arm of chromosome IV. Prior to estradiol addition, Shs1 is tagged with mCherry. Successful excision by the Cre-Lox system excised mCherry and puts GFP in frame instead. Representative images of cells prior and after excision are shown. Insets show mCherry and GFP signal at the budneck, where Shs1 is present.

(B and C) *TRP1-LYS4* distance (B) and fluorescence intensities of TetR-mCherry and LacI-GFP (C) of mother cells prior and after excision of mCherry:NAT. Statistics, graph layout and circles as in Figure 1. *p < 0.05, **p < 0.01, ***p < 0.001, non-significance not shown.

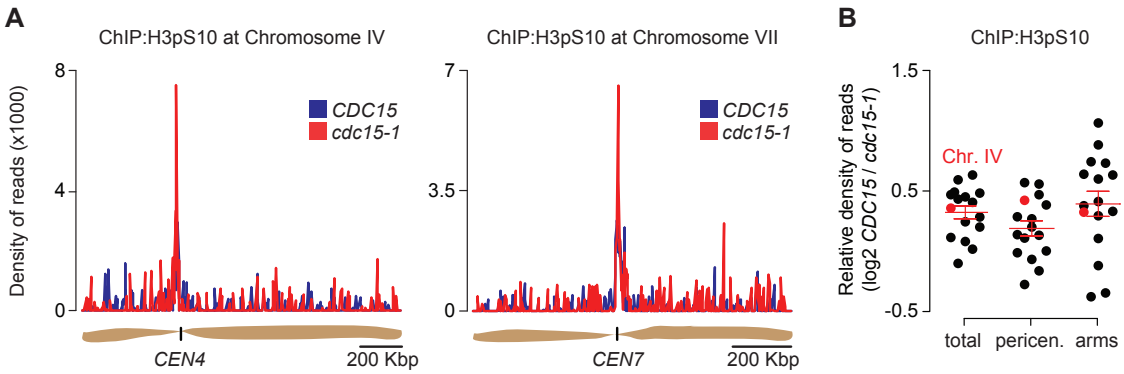

Figure S6. ChIP-Seq on H3-pS10 in *CDC15* and *cdc15-1*-Containing Cells, Related to Figure 2

(A) Detection of H3-pS10 and $H3_{total}$ by ChIP-seq at chr. IV and chr. VII in *CDC15* and *cdc15-1* cells. H3-pS10 ChIP-seq signal was normalized to total $H3_{total}$ ChIP-seq.

(B) Quantification of H3-pS10 ChIP-seq signals on whole chromosomes, pericentromeric region and chromosome arms in *cdc15-1* cells relative to *CDC15* cells. In A and B, the ChIP-seq signal corresponding to background noise coming from [H3-pS10 normalized to $H3_{total}$ ChIPs] in cells expressing H3-S10A was subtracted from the signal obtained from cells expressing *WT* H3-S10.

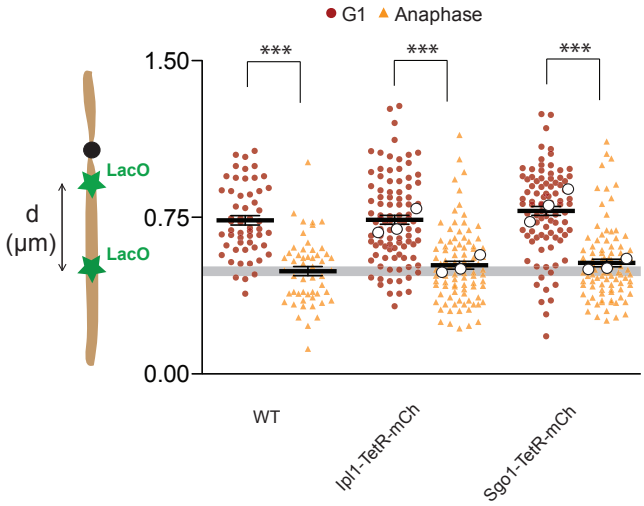

Figure S7. TetO Repeats Are Required for Ipl1- or Sgo1-TetR-mCherry Fusion Proteins to Elicit Condensation Effects, Related to Figures 4 and 6

TRP1-LYS4 distances in G1 and anaphase mother cells of a chromosome containing two LacO repeat arrays in *WT* and under expression of either Ipl1-TetR-mCherry or Sgo1-TetR-mCherry. Statistics, graph layout and circles as in Figure 1.